

APRIL 2021

M.Sc. in Engineering Physics

MUSTAFA KÖŞMAZ

REPUBLIC OF TURKEY

GAZİANTEP UNIVERSITY

GRADUATE SCHOOL OF NATURAL & APPLIED SCIENCES

IMPROVEMENT OF SIGNAL SIGNIFICANCE OF D_s^\pm MESON'S
SIGNAL VIA USING ARTIFICIAL NEURAL NETWORK

M.Sc. THESIS

IN

ENGINEERING PHYSICS

BY

MUSTAFA KÖŞMAZ

APRIL 2021

**IMPROVEMENT OF SIGNAL SIGNIFICANCE
OF D_s^\pm MESON'S SIGNAL VIA USING
ARTIFICIAL NEURAL NETWORK**

**M.Sc. Thesis
in
Engineering Physics
Gaziantep University**

**Supervisor
Prof. Dr. Ayda BEDDALL**

**Co-Supervisor
Prof. Dr. Ahmet BİNGÜL**

**by
Mustafa KOŞMAZ**

April 2021



© 2021 [Mustafa KOŞMAZ]

I hereby declare that all information in this document has been obtained and presented in accordance with academic rules and ethical conduct. I also declare that, as required by these rules and conduct, I have fully cited and referenced all material and results that are not original to this work.

Mustafa KOŞMAZ

ABSTRACT

IMPROVEMENT OF SIGNAL SIGNIFICANCE OF D_s^\pm MESON'S SIGNAL VIA USING ARTIFICIAL NEURAL NETWORK

KOŞMAZ, Mustafa

M.Sc. in Engineering Physics

Supervisor: Prof. Dr. Ayda BEDDALL

Co-Supervisor: Prof. Dr. Ahmet BİNGÜL

April 2021

62 pages

The aim of the analysis is to improve the significance of the D_s^\pm meson signal in ALEPH data which is recorded at LEP in the $D_s^\pm \rightarrow \pi^\pm + \phi$ where ϕ mesons are reconstructed from $\phi \rightarrow K^+ K^-$ decay channel. The analysis covers two phases. In first phase, reconstruction of particles in the decay channel is performed and input variables are stored to be used in classification. This phase is the machine learning part of the analysis. The second phase is the selection of an optimum algorithm for classification of signal and background. Improvement of significance of D_s meson's signal is performed after selection of the optimum algorithm and the evaluation of coefficients for relevant input variables which are stored in first phase. Classification is performed with the Toolkit for Multivariate Analysis (TMVA) which operates under the ROOT data analysis framework. TMVA includes many classification algorithms; the Boosted Decision Tree method is chosen as the optimum classification method.

Key Words: D_s^\pm Meson, Signal Improvement, ALEPH, LEP, Classification Algorithms, Hadronic Z Decays, TMVA, Artificial Intelligence, Machine Learning, Boosted Decision Trees.

ÖZET

D_s^\pm MEZONUNA AİT DEĞİŞMEZ KÜTLE SİNYALİNİN YAPAY SİNİR AĞI KULLANILARAK İYİLEŞTİRİLMESİ

KOŞMAZ, Mustafa

Yüksek Lisans Tezi, Fizik Mühendisliği

Danışman: Prof. Dr. Ayda BEDDALL

İkinci Danışman: Prof. Dr. Ahmet BİNGÜL

Nisan 2021

62 sayfa

Analizin amacı Büyük Elektron-Pozitron Çarpıştırıcısı'nda bulunan ALEPH dedektörü ile kaydedilen datalarda bulunan D_s mezonuna ait sinyalin iyileştirilmesidir. D_s mezonu, $D_s^\pm \rightarrow \pi^\pm + \phi$ bozunum kanalı vasıtasıyla yapılandırılmıştır. ϕ mezonu da $\phi \rightarrow K^+ K^-$ bozunum kanalı vasıtasıyla yapılandırılmıştır. Analiz iki kısımda incelenebilir. İlk kısım bozunum kanalındaki parçacıkların yapılandırılmasından ve sınıflandırmada kullanılacak değişkenlere ait değerlerin kaydedilmesinden ibarettir. İkinci kısım, sınıflandırmada kullanılacak optimum metodun seçilmesi ve sınıflandırmada kullanılacak değerlerin katsayılarının hesaplanması oluşturmaktadır. Sinyal iyileştirmesi sınıflandırma yapıldıktan sonra icra edilmiştir. Sınıflandırma, ROOT Data Analiz yazılımı bünyesinde çalışan TMVA analiz yazılımı vasıtasıyla yapılmıştır. Optimum sınıflandırma algoritması olarak Artırılmış Karar Ağaçları algoritması seçilmiştir.

Anahtar Kelimeler: D_s^\pm Mezon, Sinyal iyileştirme, ALEPH, LEP, Sınıflandırma Algoritmaları, Hadronik Z Bozunumu, TMVA, Yapay Zeka, Makina Öğrenimi, Karar Ağaçları.



This thesis is dedicated to all the physicists who runs after new explores...

ACKNOWLEDGEMENTS

I would like to express my greatest appreciation and thanks to my supervisor Prof. Dr. Ayda BEDDALL for being not only a tremendous mentor, but also a supportive acquaintance because of her ability to make me feel always powerful enough to achieve success.

My very special thanks go to my co-supervisor Prof. Dr. Ahmet BİNGÜL for inspiring me to improve my technical skills. And finally, we wish to thank Assoc. Prof. Dr. Andrew BEDDALL and the ALEPH Collaboration for access to the archived data since the closure of the collaboration.

TABLE OF CONTENTS

	Page
ABSTRACT	v
ÖZET	vi
ACKNOWLEDGEMENTS	viii
TABLE OF CONTENTS	ix
LIST OF TABLES	xii
LIST OF FIGURES	xiii
LIST OF SYMBOLS	xv
LIST OF ABBREVIATIONS	xvi
CHAPTER 1	1
INTRODUCTION	1
CHAPTER 2	2
THEORY	2
2.1. Explanation of Standard Model	2
2.2. Electron-Positron Collision Classification by Energy	3
2.3. Quantum Chromodynamics	3
2.4. Process from Collision to form Hadrons:	5
2.4.1. Creation of the first Quark-Antiquark Pair	6
2.4.2. Perturbative QCD	7
2.4.3. Formation of Hadrons	7
2.4.4. Transformation of Hadrons into other Particles	12
CHAPTER 3	13
LEP - ALEPH	13
3.1. Introduction	13

3.2. Large Electron-Positron Collider (LEP)	13
3.2.1. Pre-Circulation	15
3.3. ALEPH	16
3.4. Components of ALEPH	19
3.4.1. The Principal Calorimeters	22
3.4.2. The Superconducting Solenoid	24
3.5. Trigger and Data Acquisition Systems	25
3.5.1. The Trigger System	25
3.5.2. The Data Acquisition System (DAQ)	25
CHAPTER 4	28
EVENT RECONSTRUCTION AND SIMULATION	28
4.1. Introduction	28
4.2. Track Reconstruction	28
4.2.1. TPC Coordinate Determination	31
4.2.2. TPC Track Finding and Fitting	32
4.2.3. TPC-ITC-VDET Track Association	34
4.3. Event Simulation	34
4.3.1. KINGAL	34
4.3.2. GALEPH	34
CHAPTER 5	35
EVENT SELECTION	35
5.1. Data Quality	35
5.2. Hadronic Event Selection	36
5.2.1. Track Cuts	36
5.2.2. Event Cuts	37
5.3. Event Background	37
CHAPTER 6	38
ANALYSIS OF MONTE CARLO DATAS	38
6.1. Introduction	38

6.2. Modelling of Particles	38
6.3. Particle Selection Criterias	38
6.4. Selection of K^\pm candidates	41
6.5. Creation of ϕ particle	42
6.6. Selection of π^\pm particle	42
6.7. Creation of D_s particle	43
6.8. Variables of Classification	44
CHAPTER 7	46
CLASSIFICATION, TEST AND FITTING	46
7.1. Introduction	46
7.2. Separation Signal and Background	46
7.3. Testing Real Data	50
7.4. Testing Monte Carlo Data	51
7.5. Analysis for Different Energy Levels	52
7.6. Fitting	55
7.6.1. Signal Fitting	55
7.6.2. Background Fitting	55
7.6.3. Total Distribution Fitting	56
7.7. Conclusion	59
7.7.1. Outlook	59
REFERENCES	60
CURRICULUM VITAE	62

LIST OF TABLES

	Page
Table 2.1 Particle table	3
Table 7.1 Analysis in numbers	51
Table 7.2 Analysis in numbers for real data	54



LIST OF FIGURES

	Page
Figure 2.1 Coupling constant	4
Figure 2.2 Schematic diagram of the reaction $e^+e^- \rightarrow Z \rightarrow q\bar{q}$	6
Figure 2.3 Hadron production in the Field-Feynman model.	8
Figure 2.4 Electric and color field lines.	9
Figure 2.5 String hadronisation.	10
Figure 2.6 Cluster hadronisation.	11
Figure 3.1 Illustration of construction of LEP	15
Figure 3.2 LEP injection system	16
Figure 3.3 View of ALEPH	18
Figure 3.4 Configuration of the original (1991) vertex detector	20
Figure 3.5 A view of the time-projection chamber	21
Figure 3.6 The arrangement of the TPC sectors	22
Figure 3.7 ECAL modules	23
Figure 3.8 ECAL lead/wire-chamber layers	24
Figure 3.9 A simplified outline of the DAQ system	27
Figure 4.1 Data flow scheme	29
Figure 4.2 Reconstruction of tracks from coordinates in the TPC	30
Figure 4.3 Cluster example	31
Figure 4.4 TPC pad row subclusters formed by two nearby tracks	32
Figure 4.5 Helix parameters used in the TPC tracking algorithms	33
Figure 5.1 Polar angle distribution	36
Figure 6.1 Transverse impact parameter distributions	39
Figure 6.2 Longitudinal impact parameter distributions	40
Figure 6.3 Longitudinal impact parameter distributions	40
Figure 6.4 Longitudinal impact parameter distributions	41
Figure 6.5 Mass histograms of Phi	42
Figure 6.6 All histogram of D_s meson	43
Figure 6.7 Signal of D_s meson	44
Figure 7.1 Distribution of variables	47
Figure 7.2 Mass histograms of Phi	48
Figure 7.3 BDT Method's classifier response	49
Figure 7.4 Cut efficiency distribution	49

Figure 7.5	All histogram of D_s meson before TMVA	50
Figure 7.6	All histogram of D_s meson after TMVA	51
Figure 7.7	Background histogram of D_s meson (Comparison)	52
Figure 7.8	Signal histogram of D_s meson (Comparison)	52
Figure 7.9	Plotted histograms for different energy levels (1)	53
Figure 7.10	Plotted histograms for different energy levels (2)	54
Figure 7.11	Fit of signal histogram	55
Figure 7.12	Fit of background histogram	56
Figure 7.13	Total distribution fitting for Monte Carlo before TMVA . . .	57
Figure 7.14	Total distribution fitting for Monte Carlo after TMVA . . .	57
Figure 7.15	Total distribution fitting for real data before TMVA	58
Figure 7.16	Total distribution fitting for real data after TMVA	58



LIST OF SYMBOLS

D_s^\pm	Charged D_s meson
e^-	Electron
e^+	Positron
K^\pm	Charged Kaon
π^\pm	Charged Pion
ϕ	Phi
σ	Cross-section

LIST OF ABBREVIATIONS

MC	Monte Carlo (simulation)
DA	Recorded Data (real)
LEP	Large Electron-Positron Collider
ALEPH	Apparatus for LEP physics
TMVA	Toolkit for Multivariate Data Analysis with ROOT
MLP	Multilayer Perceptron
BDT	Boosted Decision Trees

CHAPTER 1

INTRODUCTION

4 fundamental forces exist in nature: strong force, weak force, electromagnetic force and gravitational force. Strong force keep together hadrons which is made up of quarks with vector boson of gluon. Electromagnetic force supplies interaction between charged particles with vector boson of photon. Weak force causes decaying a particle into another particle or particles with vector bosons of W and Z. Gravitational force causes interaction between objects which have mass. Its hypothetical vector boson is graviton, but its existence hasnt been proved yet.

The study of these 4 basic forces in nature and the knowledge about the particles arising from these forces have always been an important subject in science. High energy was needed to make these researches, many colliders were built, many crash experiments were carried out in high energy. The large electron positron collider is one of these colliders.

LEP is a circular electron-positron collider located in CERN. It was built between 1983-1988 and is the largest civil engineering project ever built in Europe [1]. Z bosons are formed from electrons and positrons that collide in LEP. Quark-antiquark pairs are formed from these subsequent Z bosons, and new hadrons and mesons form from these quark-antiquarks.

In this study, D_s^\pm mesons are reconstructed from the hadronic Z decays recorded by the ALEPH detector at LEP. In the first part of the study, $D_s^\pm \rightarrow \pi^\pm + (\phi \rightarrow K^+ K^-)$ decay channel was reconstructed by using Monte Carlo data. While the particles were being reconstructed, features that would facilitate the detection of D_s^\pm particle were determined. Later, using these detected features, a software was developed to detect the D_s^\pm meson via artificial intelligence. Later, this software tested on real data. Monte Carlo analysis was made with the events selected from the 6380794 simulation events, then the analysis performed was tested with the real data on 4179103 events. The model based on Monte Carlo is JETSET.

CHAPTER 2

THEORY

2.1 Explanation of Standard Model

This model is periodic table of particle physics and this model is product of researches which is made to explore fundamental compounds of matter and interaction between them. Standard model, also describes 3 out of 4 fundamental forces which exist in universe. There are 4 fundamental forces, strong interaction, electromagnetic interaction, weak interaction and gravitational interaction. Strong interaction(quantum chromodynamics), electromagnetic interaction and weak interaction are included. Electroweak interaction and weak interaction are unified in this model. This unification is named as electroweak interaction. Detection of gravitational interaction is harder than other interactions. Due to this hardness, gravity has not yet been included in the Standard Model.

In the Standard Model there are two groups of fundamental particles. : fermions and bosons. Fermions constitute to form atomic nuclei and they have spin of $(-\frac{1}{2})$. Bosons are interaction provider between fermions, they are force carrier particles. Spin of boson is integer, most of bosons have spin of (-1) , except graviton. This hypothetical boson have spin of (-2) . All particles in Standard Model is given in Table 2.1.

Fermions are divided into 2 groups: quarks and leptons. Quarks are building block of atomic nuclei. Protons, neutrons are made up of quarks. And mesons and baryons are also made up of quarks, mesons are formed by one quark and one antiquark, baryons are formed by three quarks or three antiquarks. Quark model was first modeled by Murray-Gell-Mann [2] and George Zweig [3] in 1964. Leptons are also fundamental particles acts with fundamental forces except strong interaction. Leptons are classified into 2 group by their electric charges : charged leptons e.g. electrons and neutral leptons e.g. neutrinos.

Table 2.1 The particles of the Standard Model.

FERMIONS		
<i>Quarks</i>		
u (<i>up</i>)	d (<i>down</i>)	c (<i>charm</i>)
s (<i>strange</i>)	t (<i>top</i>)	b (<i>bottom</i>)
<i>Leptons</i>		
e^- (<i>electron</i>)	τ^- (<i>tau</i>)	μ^- (<i>muon</i>)
ν_e (<i>electron – neutrino</i>)	ν_μ (<i>muon – neutrino</i>)	ν_τ (<i>tau – neutrino</i>)
BOSONS		
γ (<i>gamma</i>)	W^\pm (<i>W Boson</i>), Z (<i>Z Boson</i>)	<i>gluons</i> (8)

2.2 Electron-Positron Collision Classification by Energy

Electron-Positron collisions lead to different final states according to energy of collided particles.

If collision occurs at low energy, expected results are restricted by a few events. Most probably just after collision, 2 or more gamma photons are produced.[4] Energy of these photons are equal to rest mass energy of positron or electron. System has no linear momentum, so gamma rays spread out with opposite direction. With a low probability, just after collision, neutrino-antineutrino pair is created. This probability is one in ten thousand of creating gamma photons.

If collision occurs at high energy, different particles can be created just after collision. In many high energy collision experiments, J/ψ meson, ρ meson, ω meson, and D meson are observed. If energy of particle which will be collided is increased, unexperimented particles are explored. Many high energy collision experiments are made to observe dark matter.

2.3 Quantum Chromodynamics

QCD is a theory which describes interaction of quarks, with gluon. This theory is formulated similar to quantum electrodynamics except a few differences. In quantum electrodynamics, intermediate vector boson (photon) has no charge in terms of quantum electrodynamics (that is photon has no electrical charge). But in QCD, intermediate vector boson 'gluon' carry charge in terms of QCD. This charge is named as color charge. So, photons can't interact with another photon due to absence of charge, but gluons can interact with another gluon due to their

color charge. Another difference between quantum chromodynamics and quantum electrodynamics is coupling constant. Coupling constant represents strength of force in an interaction. In quantum electrodynamics formula of coupling constant is

$$\alpha = \frac{e^2}{4\pi\epsilon_0\hbar c} \quad (2.1)$$

where e is charge of electron, ϵ_0 is electrical permittivity in vacuum ($\epsilon_0 = 8.8541878128 \times 10^{-12} F.m^{-1}$), \hbar is reduced Planck constant ($\hbar = 1.05 \times 10^{-34} J.s$), and c is speed of light in vacuum ($c = 3 \times 10^8 m/s$).

In quantum chromodynamics, coupling constant's formula is:

$$\alpha_s(Q^2) = \frac{12\pi}{(33 - 2n_f) \ln(Q^2/\Lambda^2)} \quad (2.2)$$

where n_f is number of flavors in LEP(5), Q^2 is momentum transfer and Λ is obtained experimental constant which is approximately equal to 200 MeV. QCD coupling constant formula shows that, if value of momentum transfer (Q^2) increases, coupling constant decreases. That is, at high energies, quarks behave like free particle.

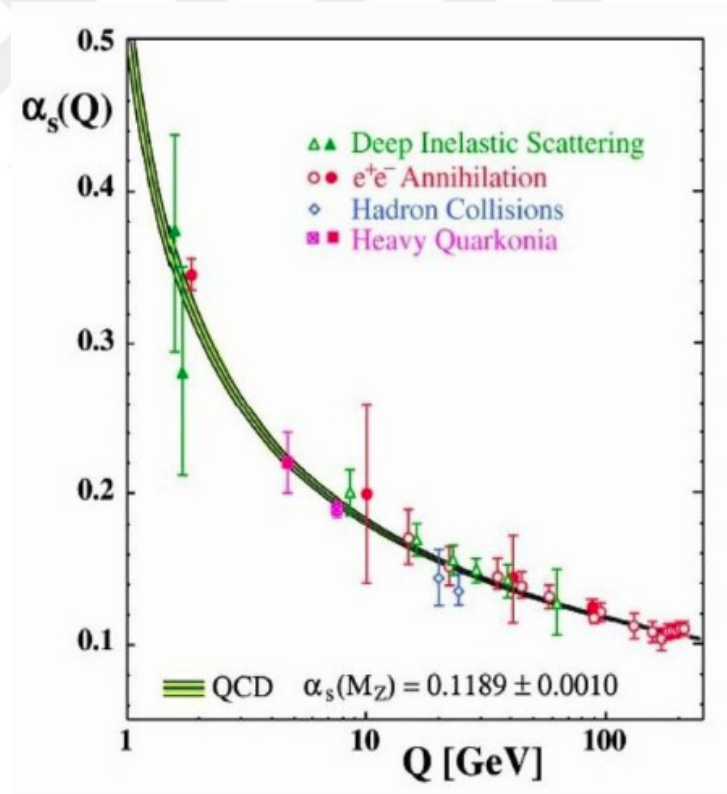


Figure 2.1 Measurement of coupling constant as a function of energy.

Figure 2.1 shows that at high energies (corresponding to small distances), the strong force's interaction strength drops to zero. At large distances, it

increases rapidly. This idea is known as 'asymptotic freedom' which has been experimentally confirmed to great precision.

2.4 Process from Collision to form Hadrons:

From electron-positron collision to creation of hadrons, whole process can be divided into 4 phase. Annihilation of electron-positron pair and Z boson production process (Electroweak phase), process of creation of quark-antiquark pair and gluons (Perturbative QCD), hadronisation process of quarks and gluons, and hadron decays.

The first phase describes the production of the initial hadronic partons, the remaining phases describe the fragmentation of these partons into the final state hadrons. These four phases are discussed below. Diagram of these process are given in Figure 2.2.

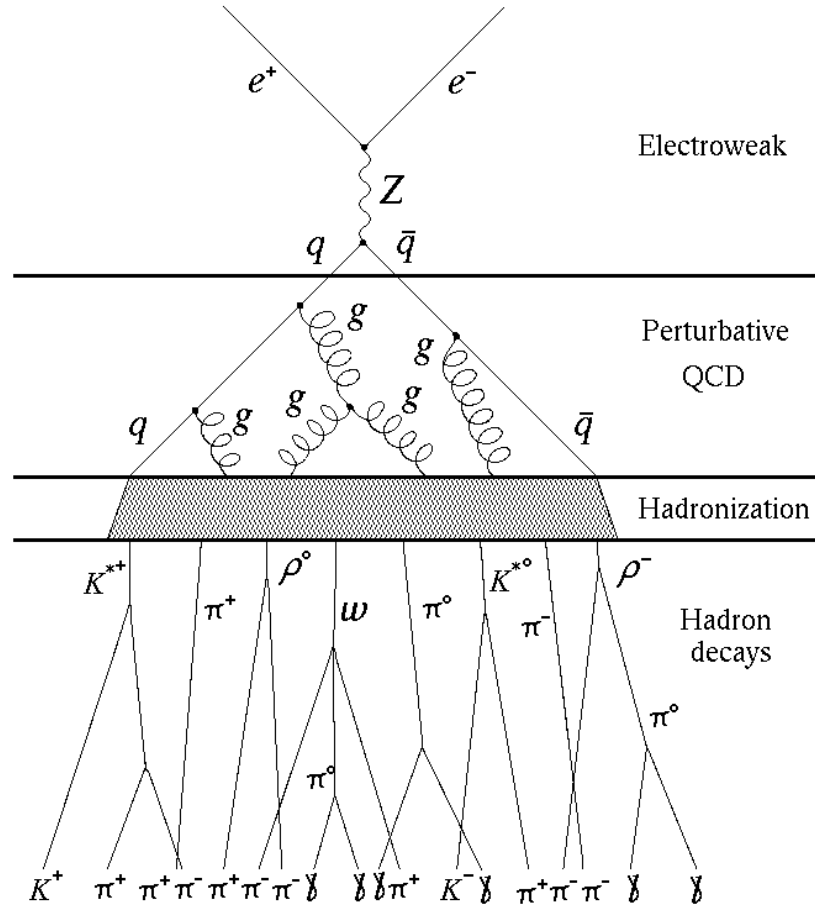


Figure 2.2 Schematic diagram of the reaction $e^+e^- \rightarrow Z \rightarrow q\bar{q}$. The development can be separated into four phases: electroweak, perturbative QCD, Hadronisation, and hadron decays.

2.4.1 Creation of the first Quark-Antiquark Pair

After collision of electron and positron, they are annihilated and Z boson is produced. Then Z boson decayed into quark-antiquark pair. This process is named as electroweak phase and it can be explained by electroweak theory. Electroweak theory is unification of strong interaction and weak interaction. This theory was put forward by Glashow [5], Weinberg [6] and Salam [7] and they awarded Nobel Prize in 1979 for this valuable contributions. By this theory, Z boson is discovered. Until Z boson is discovered, scientists had thought that intermediate boson of weak interaction is only W^\pm boson.

2.4.2 Perturbative QCD

This process is description for quark-antiquark creation or gluon emission after e^+e^- collision. In this phase, created pairs and emitted gluons have not sufficient value of strong coupling constant to form mesons or hadrons due to their high momentum. Momentum of pairs or gluons decreases with respect to time and hadronisation process begins.

2.4.3 Formation of Hadrons

Hadronisation process is starting process of creation of hadrons. In this process, perturbative QCD calculations are invalid, estimations for this process are made non-perturbatively. In this process, momentum transfer reduces, strong coupling constant raises, quarks lose their asymptotic freedom, this situation leads to prevention of exact calculation. To overcome of this problem, some hadronisation models are proposed to describe this process. There are 3 of most known hadronisation models:

- (1) Independent Hadronisation
- (2) String hadronisation
- (3) Cluster Hadronisation

Independent Hadronisation

Independent hadronisation model is proposed by R.P. Field and R.Feynmann in 1977 [8]. According to this model, hadrons are formed independently from quark-antiquark pairs. First quark-antiquark pair (q_1, \bar{q}_1) is created in color field of the initial quark q_0 which is formed just after Z boson decay. q_0 and \bar{q}_1 forms a meson together, this is primary meson. Then new quark-antiquark pair (q_2, \bar{q}_2) is created in color field of quark q_1 . Later, q_1 and \bar{q}_2 forms another meson. This process repeats until last quark is formed which has not enough energy to form a meson.

This process is illustrated in Figure 2.3.

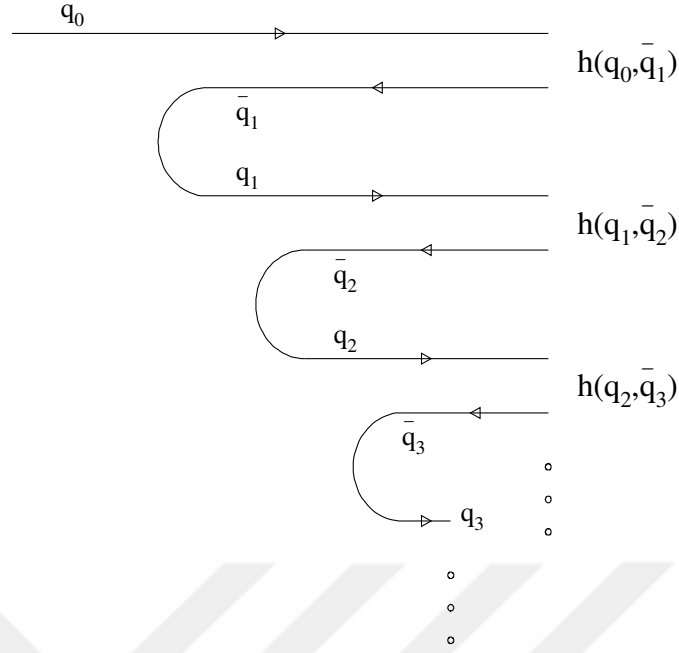


Figure 2.3 Hadron production in the Field-Feynman model.

In this model, energy of each meson which formed from quarks is expressed as function of probability. Formed meson gets an energy fraction z of the initial quark with the probability $f(z)$. This function is:

$$f(\eta) = 1 - a + 3a\eta^2 \quad (2.3)$$

where a is measured experimentally as 0.77. This model hasn't modelled hadronisation successfully in PEP & PETRA experiments, so that this model has been shelved.

String Hadronisation

QCD is guidebook of this model. An original quark-antiquark pair which produced after Z boson decay are connected each other by color flux tube. This color flux tube is similar to electric field lines between two electrically charged particles. Illustration of color flux tube and electric field lines are given in Figure 2.4

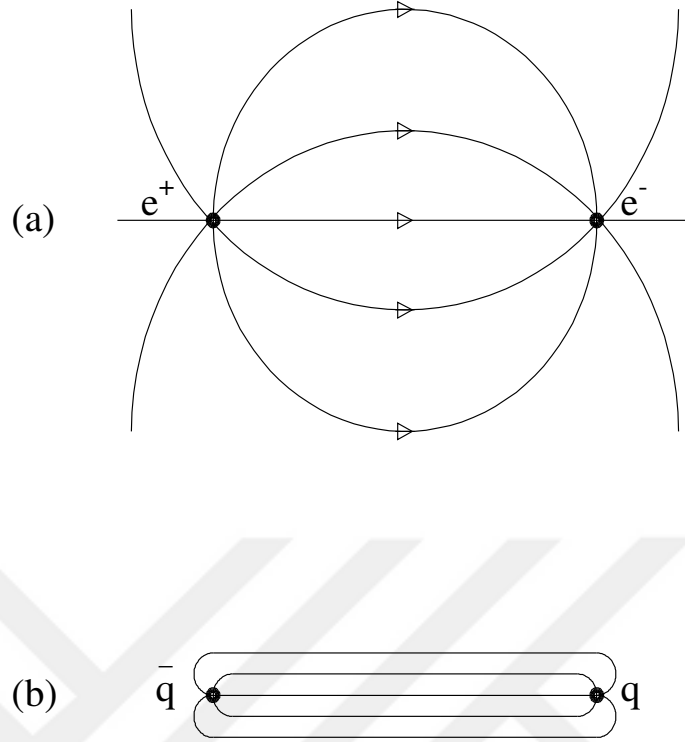


Figure 2.4 (a) The electric field lines between an electron and positron, spreading out to infinity. (b) The colour field lines between a quark and antiquark, confined in a narrow flux tube .

Transverse dimension of color flux tube is ~ 1 fm. This tube has potential which increases with respect to distance between a quark and an antiquark. That is, quarks, antiquarks and gluons can't be observed as free at large distances and below Hagedorn Temperature which is equal to 1.7×10^{-12} Kelvin. This temperature corresponds to 150 MeV energy. [9–11]

Analogy of this model with string can be explained as follows: Flux tube is analogued with string, because color flux tube is stretched between a quark and an antiquark. Gluon emission inside the color field is analogued to kink in a string. Illustration of this model is given in Figure 2.5.

STRING Hadronization

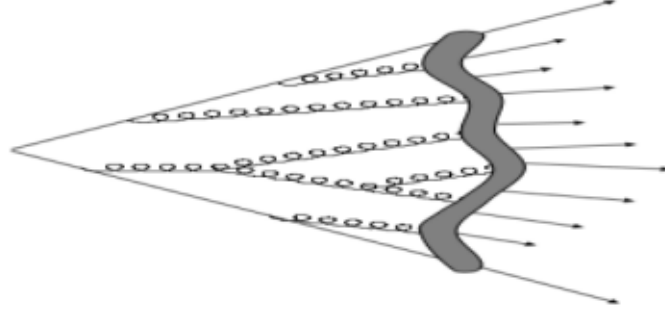


Figure 2.5 Quarks hadronize in between original quark and antiquark.

When new quark antiquark pair is created, source of energy of this new pair is mother of them. Probability of creation of new pair depends on mass of quark. This probability is named as tunneling. This probability is given as

$$\exp\left(\frac{\pi}{\kappa}(-m_q^2 - p_t^2)\right) \quad (2.4)$$

where m_q is the mass of quark, κ is string tension which is approximately equal to $\sim 1 \text{ GeV/fm}$ and p_t is the momentum of new quark. This probability states that production probability of heavy quarks, less than light quarks. Heavy quark production is expected in hard process. From heavy quarks, production of $s\bar{s}$ quark pair is suppressed by a factor of ~ 0.3 , production of $c\bar{c}$ is suppressed by a factor of $\sim \times 10^{-11}$. Baryon production can be achieved by tunneling mechanism. It is assumed that a break in the string can be caused by creation of a diquark-antidiquark pair. A suppression of baryon production comes from the assumption that the diquark mass is larger than the mass of a quark. However, the production of baryons still remains one of the least well understood aspects of particle production. Diquark-antidiquark pairs play role on baryon production. Color field of quark-antiquark pairs and diquark-antidiquark pairs are important on this process. Sum of color charges of pairs must be equal to zero, formed meson's or baryon's color charge must be zero. In this model, first mesons are formed from quark-antiquark pairs. Then from diquark-antidiquark pairs baryons are formed.

Cluster Hadronisation

This model is used in HERWIG event generator. After perturbative phase, where parton shower is stopped due to parton virtuality cut off ($\sim 0.7 \text{ GeV}$),

created gluons are split into quark-antiquark or diquark-antidiquark pairs non-perturbatively and this pairs are colorless. Then this colorless pairs which are closest in momentum space, form massive clusters are decayed, according to phase-space, into the observable hadrons. Illustration of cluster hadronisation is given in Figure 2.6.

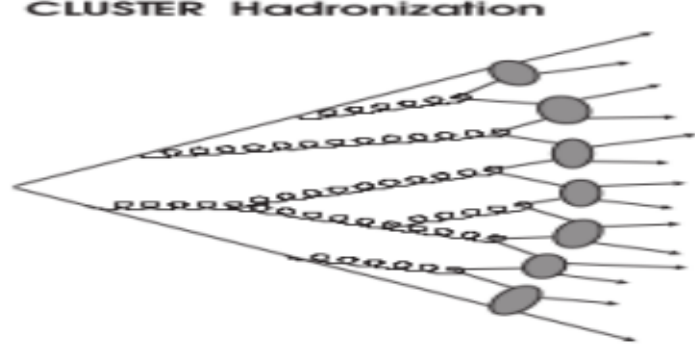


Figure 2.6 Illustration of cluster hadronisation.

After decay, most of clusters split into two hadrons that has mass above 3.65 GeV. This mass value is used in this model as an additional parameter. Clusters which have low mass can decay into single hadron in this model. This approximation for low mass clusters is introduced for treatment of this model. Baryon production is achieved by including the probability of decay of a cluster into quark and diquark (or anti-quark and anti diquark). Selection criteria of decayed hadrons depend on some properties. One of them is mass cluster. Each hadron's content which is formed after cluster decay is selected randomly from 5 quarks which is detected in LEP, with probability of their spin degeneracy for end of cluster decay. Mass of cluster must be greater than the sum of the lightest hadrons, quark content of which is randomly selected, which is product of cluster decay. Selection of hadrons are also related with their spin degeneracy. Another selection criteria is phase space weight. It is formulated as

$$W_{decay} = (2s_1 + 1) \times (2s_2 + 1) \times p_{cm} \quad (2.5)$$

where s_1 and s_2 are spin values of 2 daughter hadrons, p_{cm} is momentum in center of mass. W_{decay} determines acceptability of selected cluster. If cluster selection is rejected, new quark flavours are reselected.

2.4.4 Transformation of Hadrons into other Particles

Finally, hadrons which created in hadronisation process decay into mesons and this mesons decay into another mesons according to their lifetime. Pion is most frequently detected particle on detector level, number of pions which comes from directly hadronisation is less. Pion is the particle most frequently detected on detector level, number of pions which comes from directly hadronisation is less relative to whole detected number of pion. Contrarily rate of detected particle which directly comes from hadronisation is high, so inclusive resonance studies gives information about the dynamics for fragmented particles. However, inclusive resonance distributions are sensitive to heavy flavour decay tables. The vector resonances are, in addition, sensitive to tensor production; tensors occupy phase-space which would otherwise be occupied by vectors. In this thesis, inclusive production of D_s meson is studied, from the decay channel of $D_s^\pm \rightarrow \pi^\pm + [\phi \rightarrow K^\pm]$. Also, this study provides a test of fragmentation process which is implemented in the JETSET, PYTHIA and HERWIG Monte Carlos.

CHAPTER 3

LEP - ALEPH

3.1 Introduction

Detecting particles which moves as fast as light is very hard. Particles smallness make detection harder. To detect these particles, very developed hardwares are required. In LEP, very developed hardwares such as tracking chambers, calorimeters, and supermagnets are used to detect W^\pm and Z bosons, other particles and decay channels, energy and momentum of particles. Each of these hardwares are member of a big detector : ALEPH. ALEPH stands for Apparatus For LEP Physics. There are other 3 huge detectors in LEP, each of them records event after collision. Other three detectors are DELPHI, L3 and OPAL. DELPHI stands for Detector with Lepton, Photon and Hadron Identification. OPAL stands for Omni-Purpose Apparatus for LEP, it is used to make high precision of the Z Boson lineshape. In this chapter, LEP, ALEPH and its parts are explained.

3.2 Large Electron-Positron Collider (LEP)

LEP is one of the biggest lepton accelerators. To obtain more realistic results about electroweak theory, W^\pm and Z bosons, an accelerator is required. After specifying its design parameters, it is started to be built on 1983, in Geneva, Switzerland. With large circumference, detectors with advanced technology, LEP was very expensive accelerator. Every parameter for building of this collider is considered meticulously, so that this collider is encapsulated to underground to get rid out of environmental noise which affects colliding particles. The machine enclosed in a tunnel situated between 50 to 170 meters below ground. First lepton beam was circulated in 14 January 1989, and first event was recorded on 13 August 1989 by OPAL detector. Later experiments each recorded around

30 000 Z particles, enough for the first data analysis to get under way. On 13 October 1989, ATLAS, OPAL, L3 and DELPHI collaborations working on the LEP experiments presented their first results at a seminar organised at CERN. Then all of them confirmed existation of three neutrinos , and hence there are only three generations of matter particles. At 2 November of 2000, LEP was shut down and then dismantled in order to make room in the tunnel for the construction of the Large Hadron Collider (LHC). Electron bunches and positron bunches travel inside an evacuated pipe, along enormous circumference of LEP which is equal to 27 kilometers. In this travel, each bunch was kept together and orbitted by electromagnets; 1320 quadrupole and sextupole magnets focus the particles in all the sections creating a luminous region (the beam spot) of length 18 mm (in the z-direction), and cross-section with $\sigma_x \approx 0.25$ mm, and $\sigma_y \approx 0.015$ mm. The luminosity of LEP is $10^{32} \text{ cm}^{-2} \text{ s}^{-1}$, producing Z bosons at a rate of 1 Hz (on peak). 3392 dipoles bend the beams around the curved sections. To gain energy instead of energy loss which is due to synchrotron radiation, 128 copper radio frequency (RF) cavities are used. In LEP, electrons and positrons circulate whole circumference, due to this circulator leptons loss energy. Amount of loss is equal to emitted synchrotron:

$$P = \frac{(4 \times \pi)(e^2 \times \beta \times E^4)}{3 \times (m^4 \times c^8 \times r)} \quad (3.1)$$

To get rid out of energy loss, large radius is required, so that circumference of LEP is large.

In first collisions, number of collided bunches are 4 for each lepton. Number of bunches is incremented to 8 in 1992. And finally bunches are collided as a crowded set. Like incrementation in number of bunches in LEP, energy were incremented also. From 1989 to 1995, collision was made at total center of mass energy of 91.2 GeV. And from 1995 to 2000, amount of total center of mass energy is increased to 140 GeV [12] to observe on-shell W^\pm bosons.

With a circumference of 27 km, the LEP collider at CERN is the largest e^+e^- collider ever built. LEP operated at the Z peak between 1989 and 1995 with e^+e^- collisions around the Z resonance (91.2 GeV center of mass) for the four LEP experiments ALEPH, DELPHI, L3 and OPAL, Figure 3.1. The collider was upgraded in 1995 and ran until 2000 in its second phase where the collision energy was doubled in order to produce pairs of on-shell W^\pm bosons.

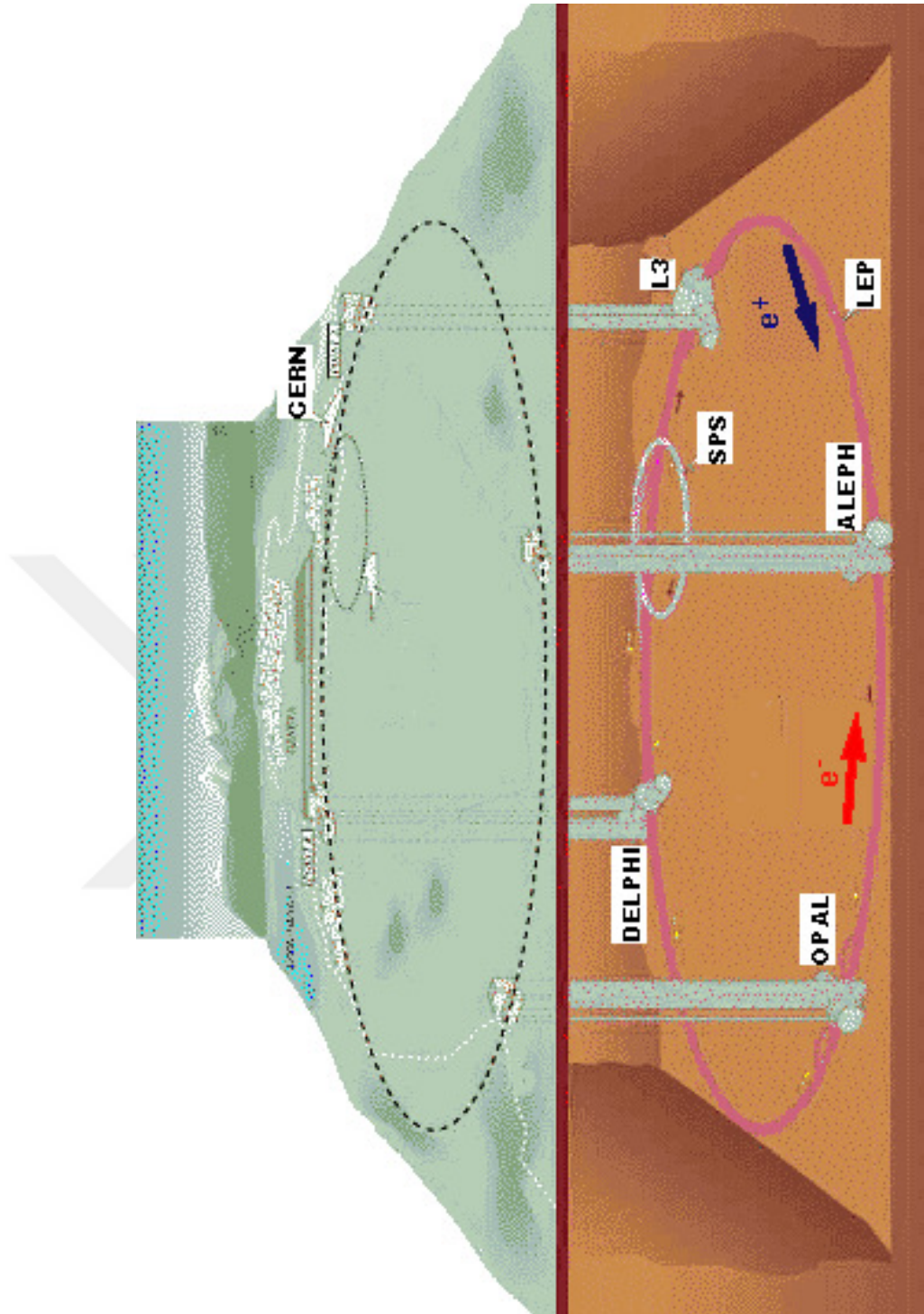


Figure 3.1 Illustration of construction of LEP.

3.2.1 Pre-Circulation

To gain large amount of speed to leptons, their speed must be increased before their circulation on LEP's circumference. This is possible only after some

processes, by using synchrotrons. Synchrotron is cyclotron wherein the strength of magnetic field increases with the energy of particles to maintain their orbital radius constant. [13] First process is sending leptons to Electron Positron Accumulator (EPA). Electrons (from an electron gun) and positrons (from a tungsten converter) are accelerated to 600 MeV by the LEP injection linac (LIL) and then they are stored in EPA. After number of stored lepton is sufficient, stored leptons are transferred into Proton Synchrotron and their acceleration are increased to 3.5 GeV, this is second process. And then accelerated lepton is transferred into Super Proton Synchrotron to complete last process. In SPS, leptons are accelerated to 20 GeV after that leptons are circulated around LEP's circumference. And finally, circulated particles are collisioned inside detectors to observe resultant particles.

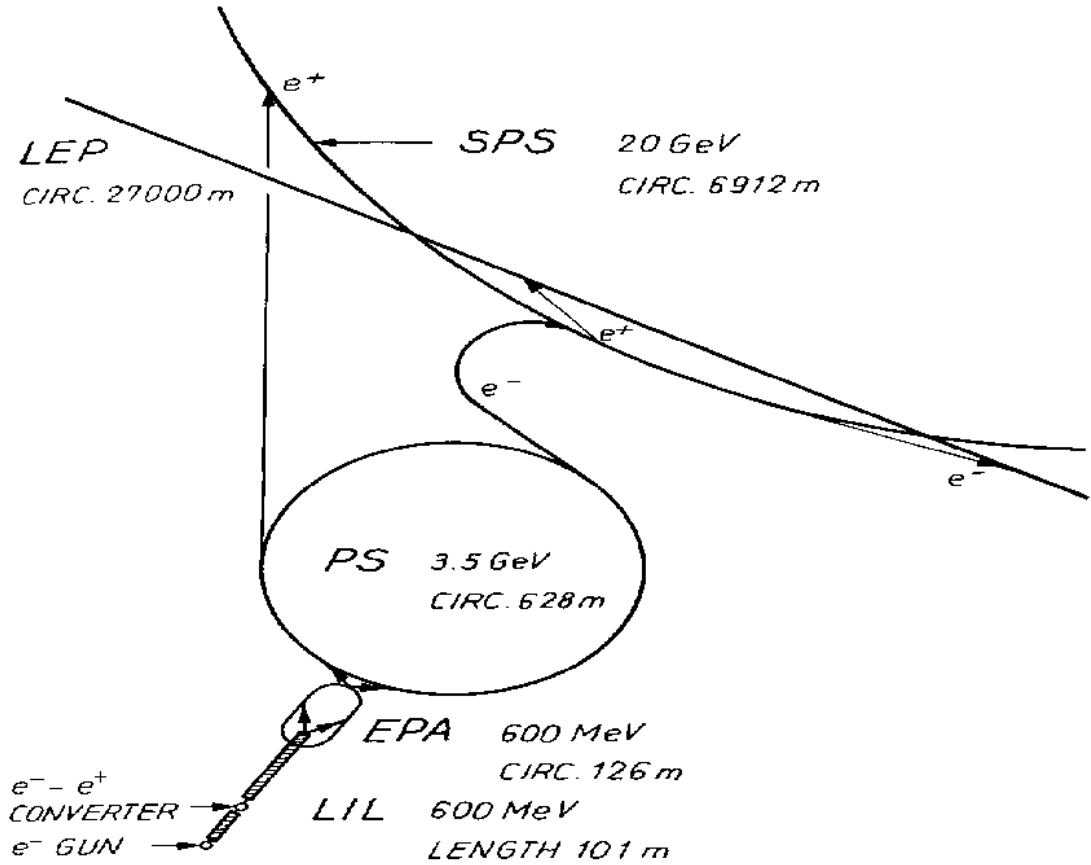










Figure 3.2 Before circulation leptons are accelerated to reach sufficient energy.

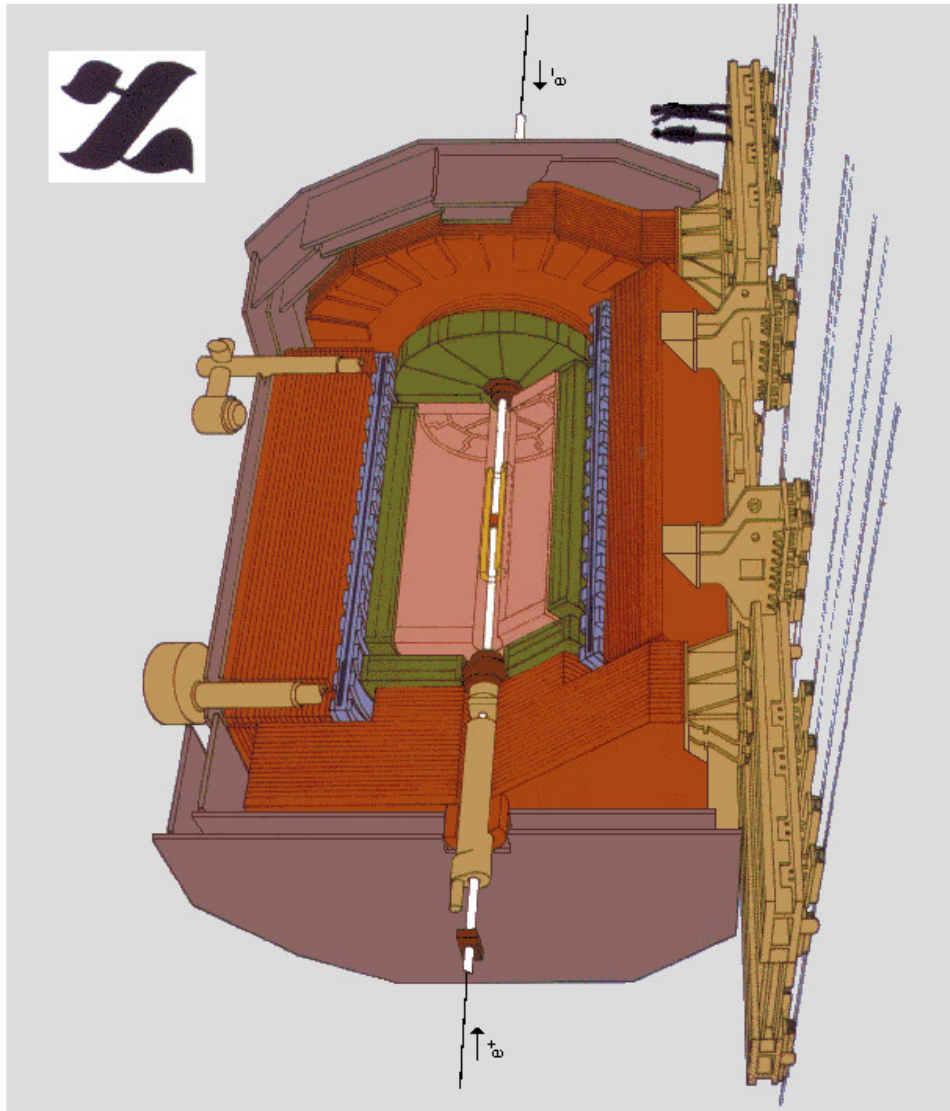
3.3 ALEPH

ALEPH was measured the events created by electron positron collisions in LEP, at first (1989 to 1995) in the energy range of the Z particle (around 91 GeV)

and later (1995 to 2000) above the threshold of W pair production (up to 200 GeV). [14] ALEPH first measured events in LEP in July 1989. This experiment was a large collaboration of several hundred participants from around the world. ALEPH was closed in 2004.

Detector is designed for multiple purposes : First purpose is to measure particles momenta. Second purpose is to measure energy of every particles either neutral or charged. This is achieved by using calorimeters. Also, to know about flavour of three leptons, and to measure distance of short-lived particles is purposes of designing of this detector. Detector design is suitable for recording events at a wide angle. Both cartesian coordinate (x,y,z) and cylindrical coordinate $(r,\phi,theta)$ were used in ALEPH. ALEPHs design was depend on cylindrical arrangement of units. In the most inner of detector, a long beam pipe was placed, which was road for electrons and positrons. Long beam pipe is surrounded by inner tracking chamber. Out of inner tracking chamber is surrounded by Time Projection Chamber. Time Projection Chamber is surrounded by a superconducting coil. This coil creates a magnetic field of 1.5 Tesla and its length is 6.4 m, and its dimension is 5.3 m. Outer side of coil is surrounded by electromagnetic calorimeter and electromagnetic calorimeter is surrounded by hadron calorimeter. And luminosity monitors are used to measure cross-section.

Vertex Detector	Inner Tracking Chamber	Time Projection Chamber	Electromagnetic Calorimeter	Superconducting Magnet Coil	Hadron Calorimeter	Muon Chambers	Luminosity Monitors
							



The ALEPH Detector

Figure 3.3 View of ALEPH detector.

3.4 Components of ALEPH

VDET (The Vertex Detector)

This detector records informations about particles which are created after collision. These particles collide on to this detector. And tracking information of incoming particle is recorded by this detector. By help of these informations, decay channels can be reconstructed. There are 96 silicon wafers in this detector. Each of wafers has 5.12 cm width, 5.12 cm length and 0.03 cm depth. Wafers arrangement is cylindrical. Technical drawing of this detector is given in Figure 3.4.

ITC (Inner Tracking Chamber)

Inner Tracking Chamber is positioned around of vertex detector and surrounds it. There are drift cells which are positioned in this chamber. By help of these drift cells, position of tracks can be measured in cylindrical coordinate.

The ALEPH Vertex Detector

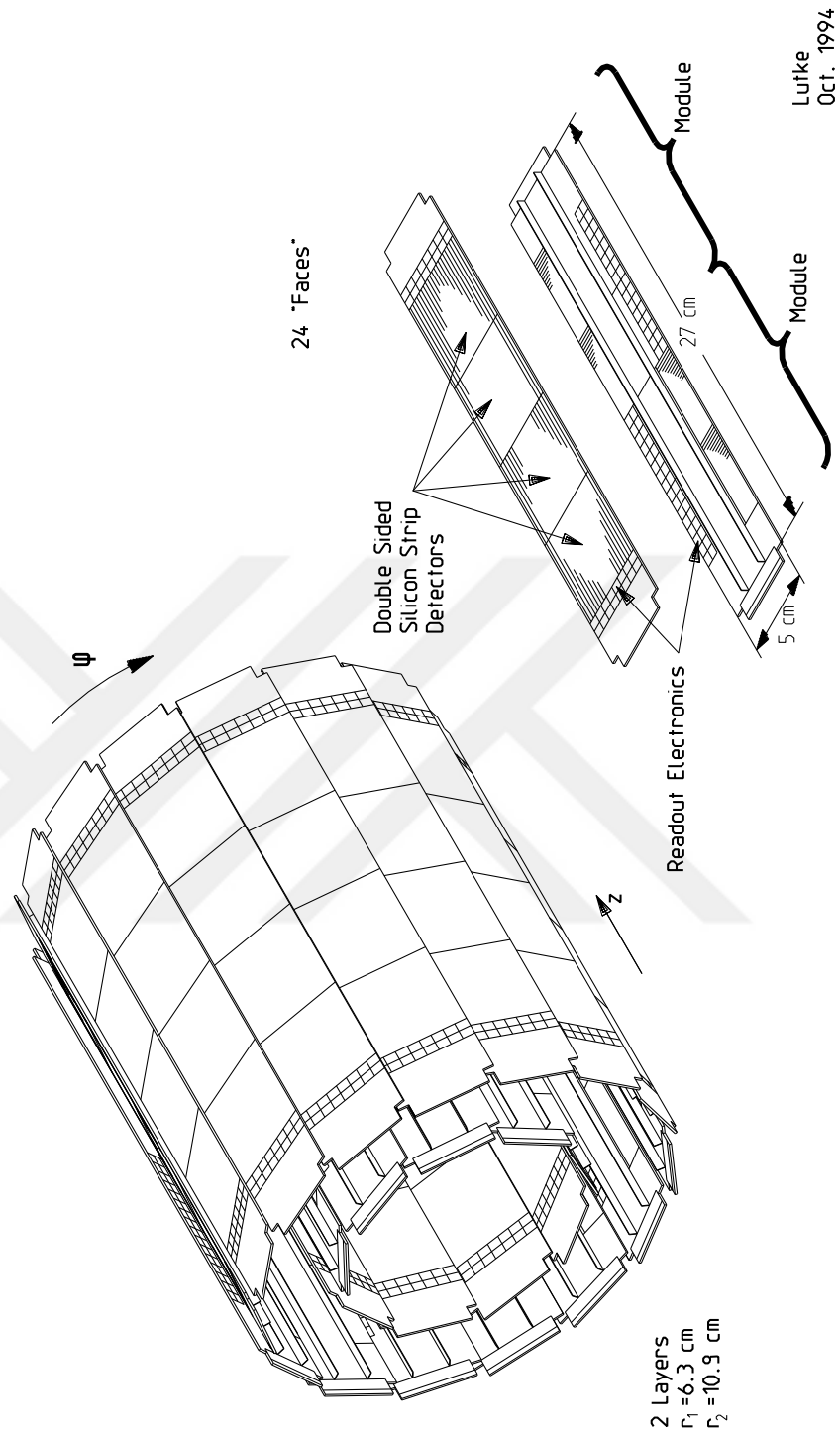


Figure 3.4 Configuration of the original (1991) vertex detector. The VDET is very close to the beam pipe in order to identify very short-lived particles (such as τ leptons and B mesons) with a high resolution position. This detector consists of two concentric arrays of silicon wafers surrounding the beam pipe.

TPC (Time Projection Chamber)

Inside of TPC is filled with gas, and there is a midriff in center of TPC. Gas in TPC is ionized when charged particle move inside it. Ionisation cause to pulse and by help of this pulse, position of charged particle can be measured in cylindrical coordinate. Front and back end of TPC is made up of wire chambers and cathode pads. Dimensions of cathod pads are $6.2 \text{ mm} \times 30 \text{ mm}$ ($r\delta\phi \times \delta r$) and the pad pitch in azimuth is 6.72 mm. The resolution in azimuth coordination is $\sigma_{r\phi} = 180$ micron at zero degrees angle of crossing. The z space resolution is 1.2 mm and 0.8 mm for wires and pads respectively. Arrangement of TPC is given in Figure 3.5

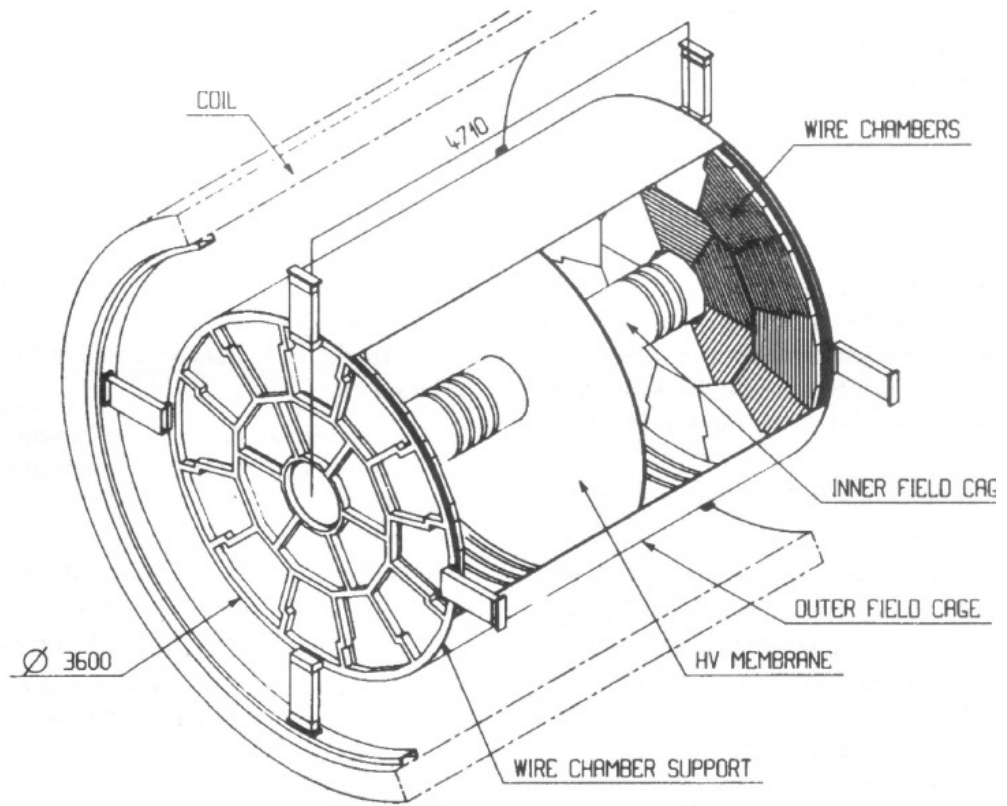


Figure 3.5 A view of the time-projection chamber.

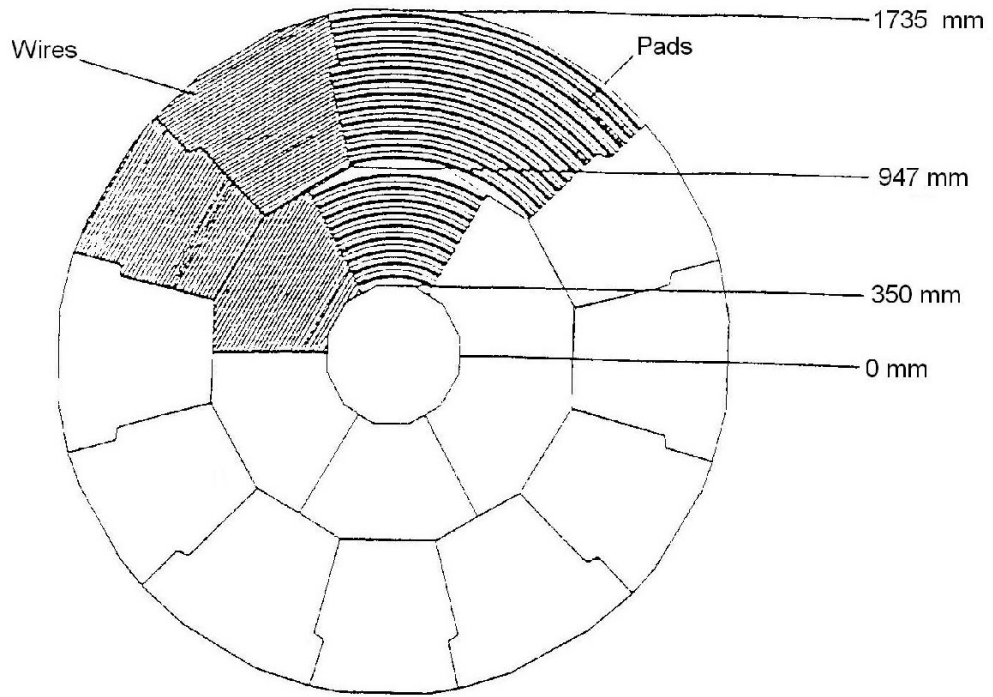


Figure 3.6 The arrangement of the TPC sectors.

3.4.1 The Principal Calorimeters

Special calorimeters are used in ALEPH to measure coordinate of energy and position of secondary and tertiary particles. Energy of these particles are absorbed by calorimeters. Absorbed energy is processed and information for energy and position is extracted. Several calorimeters are there to measure of various type of secondary and tertiary particles

The Electromagnetic Calorimeter (ECAL)

This calorimeter is designed to identify photons, electrons and neutral pions and this calorimeter surrounds TPC. Structure of ECAL is the similar to the structure of a barrel. Front-end and back-end of ECAL is made up of modules which is arranged circularly. Each modules cover $\pi/6$ radians. There are 45 lead wire chambers in this modules. Position and energy coordinates of particle showers are read by cathode pads which are part of wire chambers. The angular resolution is calculated for the ECAL as

$$\sigma_{\theta,\phi} = \left(\frac{2.5}{\sqrt{E}} + 0.25 \right) \text{ mrad} \quad (3.2)$$

where E is measured in GeV.

Schematic view of ECAL and technical drawing of cathode pads are given in Figure 3.7 and 3.8

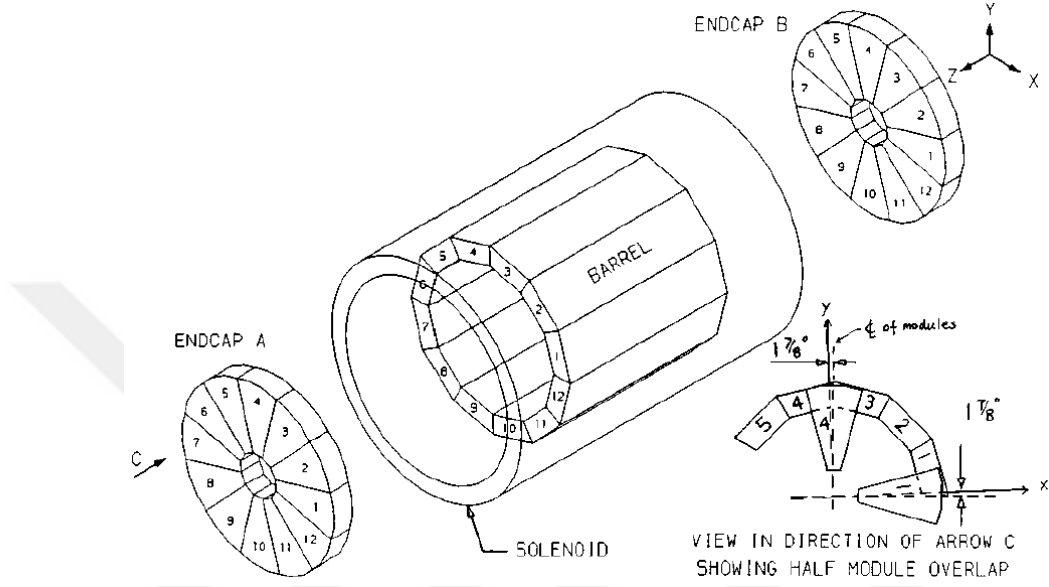


Figure 3.7 Schematic view of the ECAL modules.

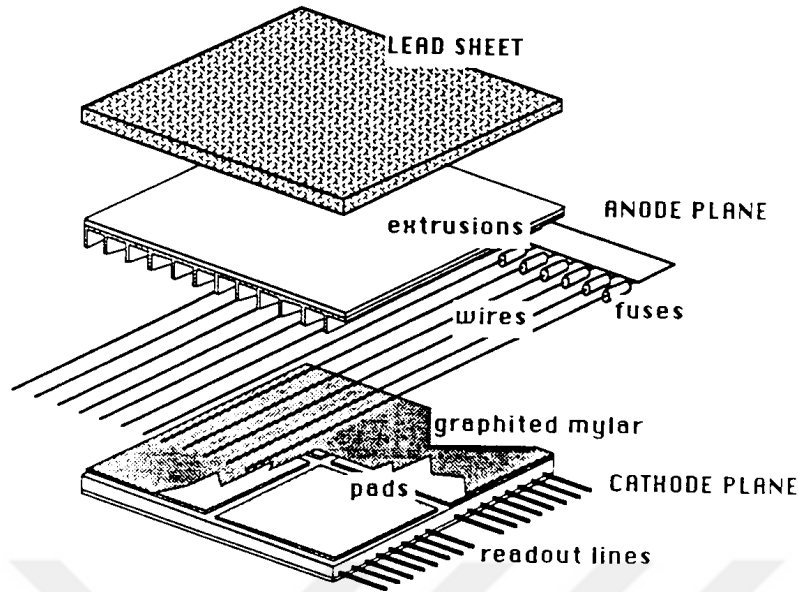


Figure 3.8 ECAL lead/wire-chamber layers.

The Hadron Calorimeter (HCAL) and Muon Chambers

It is used to determine hadronic energy deposition with ECAL and contributes to identification of muons. It is composed of 23 layers of plastic streamer tubes which are separated by 5 cm iron slabs, giving a total of about 7.2 interaction lengths at 90 degrees. HCAL consists of 36 modules. 24 of modules are in a barrel, 6 of modules are in both front-end and back-end of HCAL. Muon chambers are formed with two double layers of streamer tubes and it is positioned outside of HCAL. Muon chambers are used for identifying muons with HCAL.

3.4.2 The Superconducting Solenoid

This super solenoid magnet, helps to identify sign of charged particles. It carries 5000 A of current and it has 1.5 T of magnetic field. To prevent overheating , this magnet is cooled with liquid helium.

The Silicon Calorimeter

This calorimeter has important role on measurement of luminosity Silicon and tungsten layers are used for sampling particle showers which are created by Bhabhas. These layers are arranged meticulously, angle of incident particles are calculated with a polar resolution of 0.15 mrad

The Luminosity Calorimeter

Its design is similar to ECAL. LCAL consists of 38 modules and LCAL has an energy resolution of $\sim 0.15/\sqrt{E} + 0.01$, where E is measured in GeV.

BCAL

Bhabha Calorimeter supplies online luminosity monitoring. BCAL consists of tungsten and plastic scintillators.

3.5 Trigger and Data Acquisition Systems

3.5.1 The Trigger System

To select exact e^+e^- interactions, 3-level trigger system is performed. In first level, energy level in HCAL and ECAL, number of track candidates in ITC number of Bhabha events in SiCal and energy in whole detector is controlled. If conditions are satisfied in this level, Time Projection Chamber is controlled for existence of charged particles, this is second level. If charged particle is detected, then exact e^+e^- interactions are separated from other interactions by using software as third level.

3.5.2 The Data Acquisition System (DAQ)

Aim of DAQ is to process electronic signals which come from detectors and create understandable data from this signals. Extracted data is used to reconstruct collision event. The main steps in the data flow are as follows:

- (1) Trigger supervisor receives signal from module synchronously with bunch

crossing .

- (2) The trigger supervisor send received signal to the readout controllers (ROCs) which, for most of the subdetectors, digitisation is started in the front-end electronics. After formatting data and making calibrations results are saved to ROCs' output buffers.
- (3) The Level 1 and Level 2 trigger decisions are made and transmitted to the ROCs. If a trigger is rejected the digitisation process is cancelled and the ROCs are initialised for the next event. If a trigger is accepted at Level 2 then the whole event is digitised.
- (4) Digitisation is made, each ROC sends a signal to the corresponding subdetector event builders (EB) receive signal from associated ROCs. EB processes data and store it in output buffer.
- (5) Data is received and read by Main Event Builder. Event is assembled by Main Event Builder. After Level 3, trigger analysis is performed for the test. A Level 3 *yes* decision results in the event being written to a disk and then to tape. The data are now available for event reconstruction, this is the subject of the next chapter.

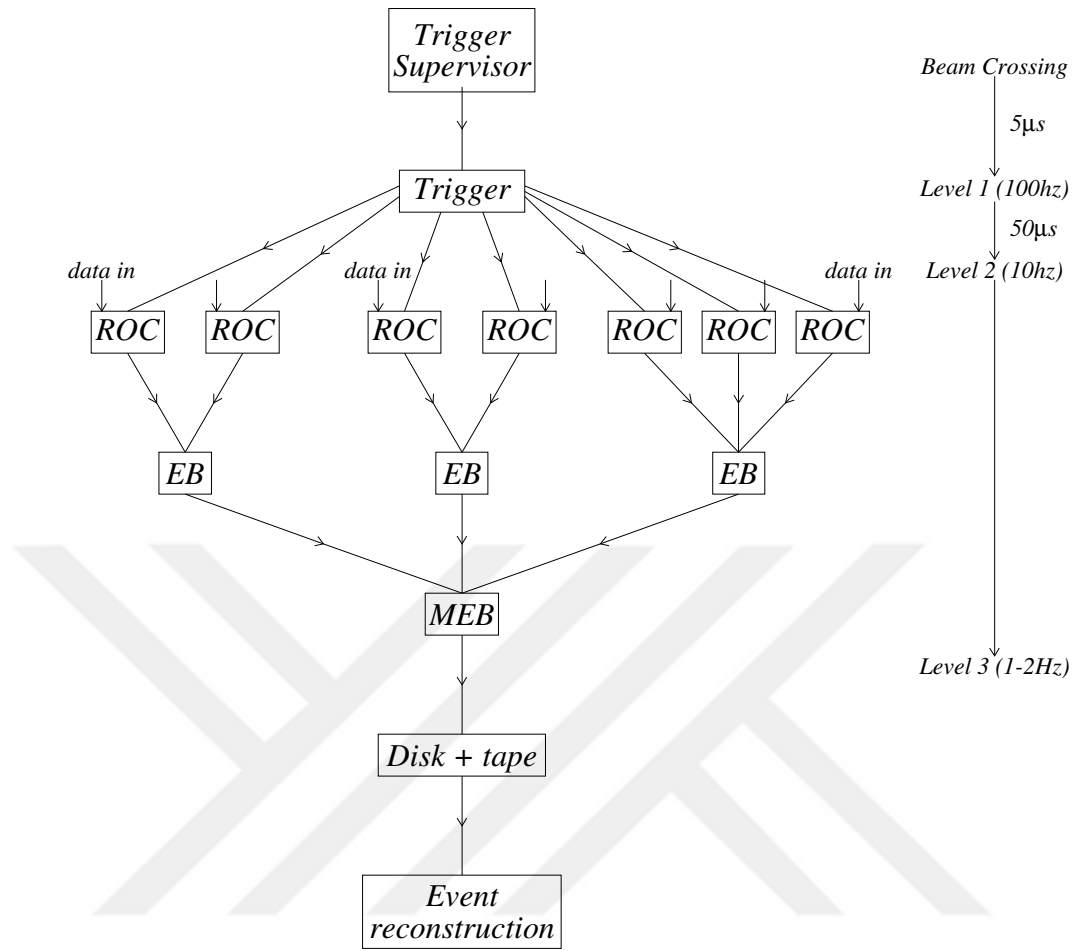


Figure 3.9 Organization scheme of Data Acquisition System.

CHAPTER 4

EVENT RECONSTRUCTION AND SIMULATION

4.1 Introduction

Stored collision data is reconstructed by JULIA program. Tracking and calorimeter reconstruction is performed on both real and simulated data. The results from JULIA are formed into BOS banks and written to Production Output Tapes (POTs) and then to Data Summary Tapes (DSTs) ready for physics analysis; DSTs contain almost all the information from the POTs, but with non-interesting events (i.e. noise and background) removed. More compact form of data is Mini-DST. By help of time-consuming algorithms, this form of data can be analysed faster. The processes described in this chapter have already been applied by ALEPH, the current study performs analysis on datasets derived from ALEPH archived data.

4.2 Track Reconstruction

Tracks are produced by fitting a helix to coordinate informations in three dimensions. Trajectory of charged particle is similar to a helix, so coordinate informations are fitted a helix. Trajectory of particles in x-axis and y-axis is curved. In Figure 4.2, sample of track reconstruction from coordinate information in TPC is given.

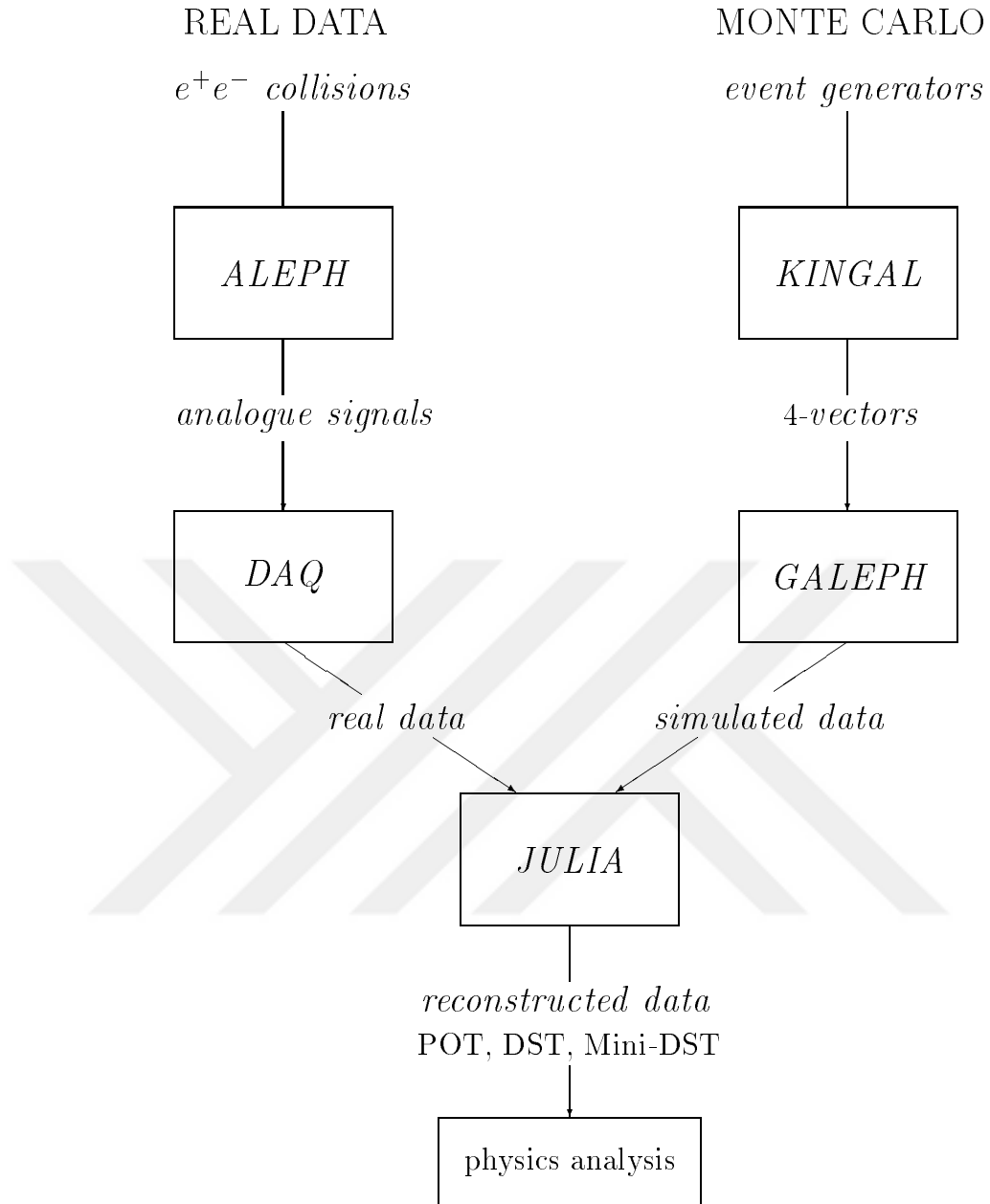


Figure 4.1 Illustration of data flow process in ALEPH from begin to end.

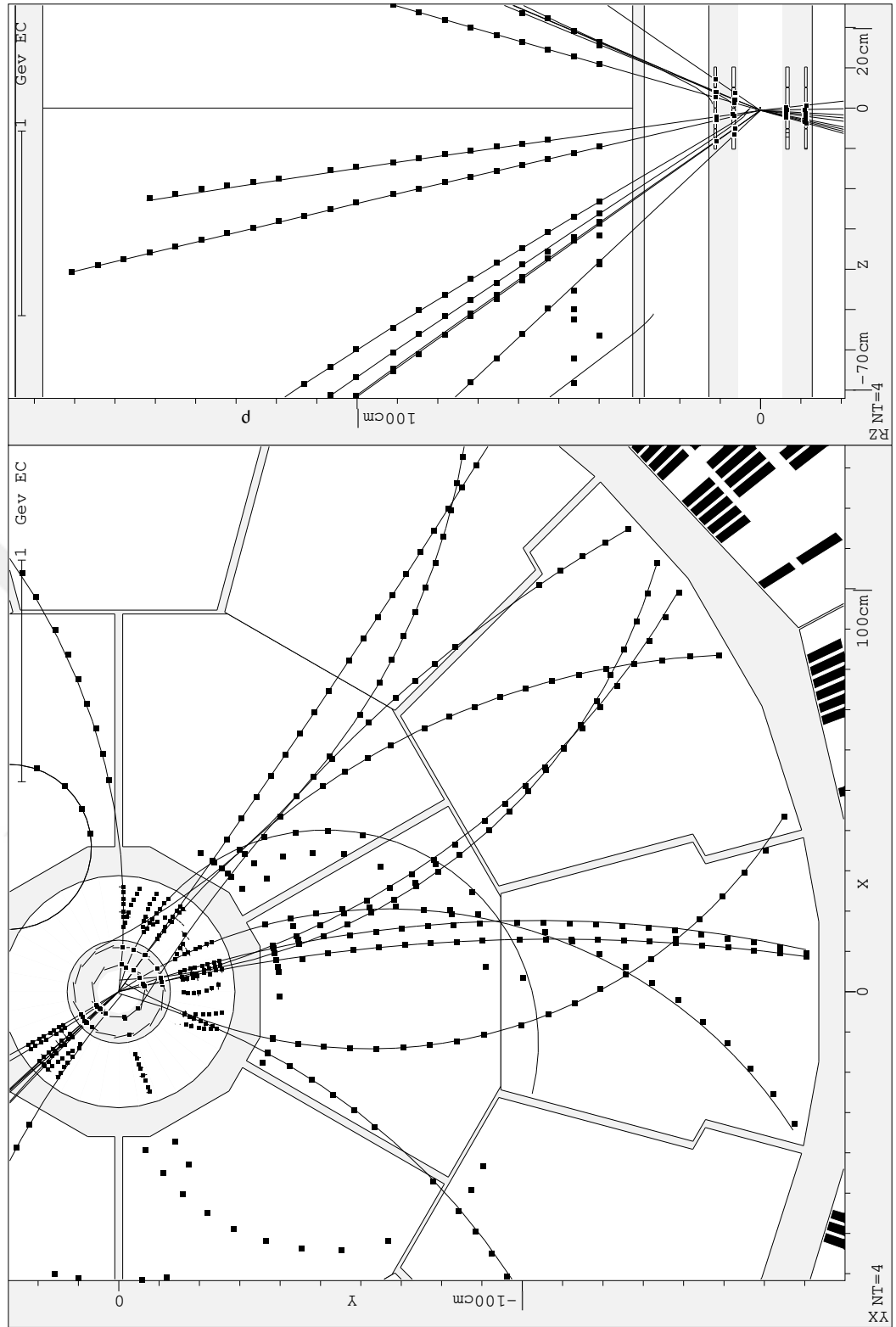


Figure 4.2 Tracks are reconstructed by help of Time Projection Chamber.

4.2.1 TPC Coordinate Determination

Pads which are part of Time Projection Chamber have important role on coordination determination. If a particle hit to pad, hitting time, number of pad and time length of hitting is recorded and used to determine coordinate of particles. Arrangement of pads are related with the number of pads.

Clusters and Pulses

To determine coordinate, clusters are formed from informations which are collected by TPC. This cluster can be assumed as two column of data. One of column includes information of pad number, and the other includes drift time(time duration of hitting). Sample of cluster is given in Figure 4.3,

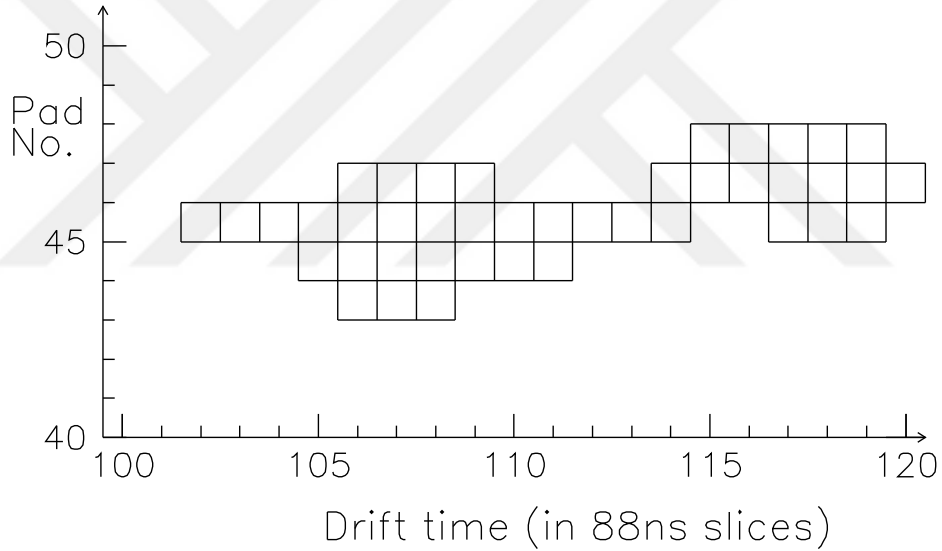


Figure 4.3 Example of clusters.

Clusters are classified in order to hit number and cluster length.

Subclusters and Subpulses

To perform more efficient analysis, formed clusters are divided into subclusters. Each subcluster includes different drift-time information which is recorded by different pads. To understand source of peaks, or separate peaks of

different particles, charge profile of peaks are investigated. Illustrated subcluster vs subpulse graph example is given in Figure 4.4.

Coordinates

Subcluster are used to calculate cylindrical coordinate. For the $r\phi$ coordinate the sub-pulse charge estimator is used. The z coordinate is calculated using both the charge estimator and the time estimator.

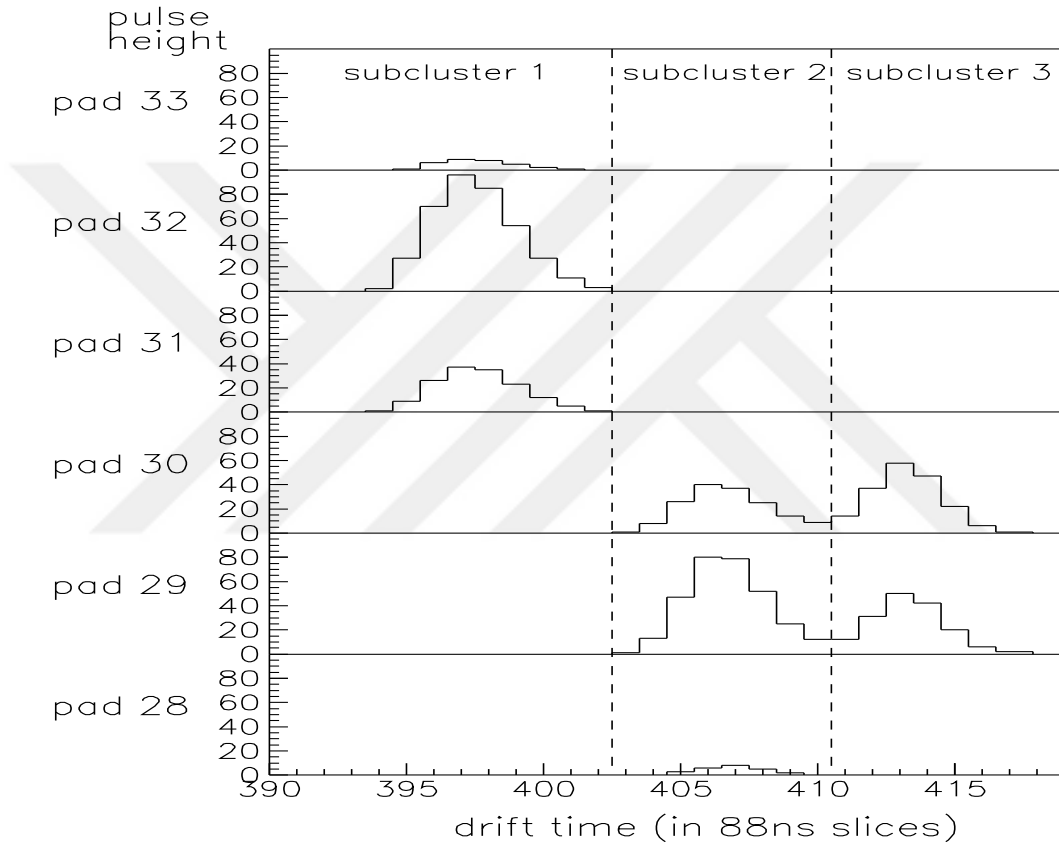


Figure 4.4 An example of a complex cluster and how the reconstruction program has broken it down into three contributions from which three individual coordinates can be calculated.

4.2.2 TPC Track Finding and Fitting

TPC coordinates which are in shape of an arc chains that are determined to belong to the same helix (e.g. multiple arcs of a spiral) are linked together into a single ‘track candidate’. To account for multiple scattering, the coordinate error

estimates are increased in accordance with the distance from the track origin. If an acceptable fit is not obtained, then up to two points are removed from the fit, corresponding to those that contribute the most to the χ^2 of the overall fit. If this does not result in an acceptable fit then a search is made for a kink in the track candidate, and if one is found the track is split. If no significant kink is found then a search is made for bad points by fitting a track candidate with one point at a time removed. If none of these methods leads to a good fit the track candidate is kept without modification. Details of the algorithms used to find and combine the chains into track candidates can be found in [15].

The track finding efficiency in the Time Projection Chamber is studied using Monte Carlo. In hadronic Z decays, about 99% of tracks crossing at least four pad rows are reconstructed successfully.

The five helix parameters given in Figure 4.5 can be found by fitting a helix function to the pad coordinates.

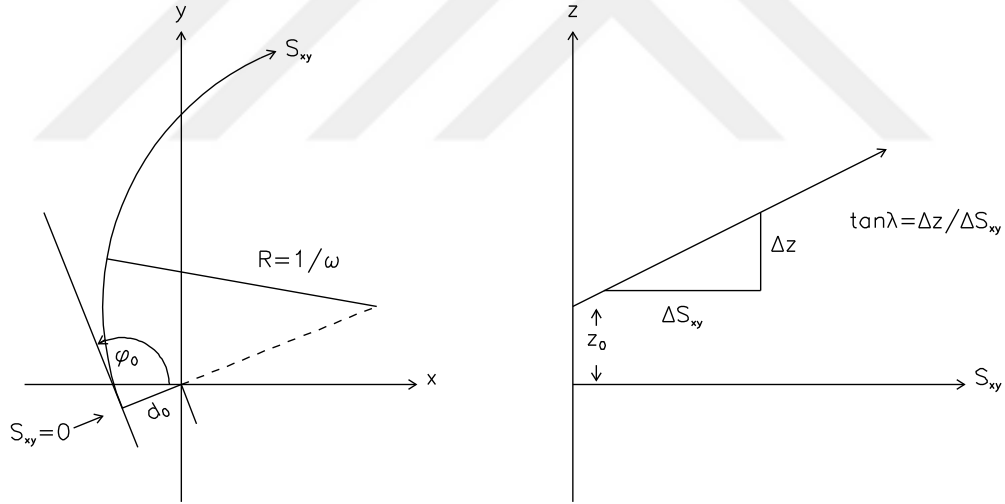


Figure 4.5 Helix parameters used for track finding algorithms in TPC.

A circle fit performed in $x - y$ plane results in ω (defined as inverse radius of curvature), d_0 , and ϕ_0 (the angle of emission in $x - y$ plane). A linear fit in the s_{xy} - z plane yields z_0 (the z coordinate at the closest approach to the z axis) and $\tan \lambda$ (representing the tangent of dip angle). The circle fit parameters are used to calculate the values of s_{xy} .

4.2.3 TPC-ITC-VDET Track Association

ITC and VDET coordinates are in relationship with TPC coordinates. Depending on number of hits in ITC, ITC and VDET coordinates are merged with TPC's and fit is performed on whole coordinates.

4.3 Event Simulation

After millions of events are generated with JETSET [16] software and formatted with KINGAL program, first phase of simulation is done. For second phase, detectors are created virtually with GALEPH program and measurement with these virtual detectors is performed on particles which are created with JETSET and formatted with KINGAL.

4.3.1 KINGAL

Generated events with JETSET software are given into KINGAL as input, and output is given as 4-vector kinematics for inputs. So, generated events are formatted as usable for simulation in virtual detectors.

4.3.2 GALEPH

Detectors are simulated with GALEPH for investigating effect of particles on detectors. Every properties of detectors are taken into account for simulation, even type of material and digitization of pulses. So, designs for detectors can be optimized.

CHAPTER 5

EVENT SELECTION

There are two considerations in choosing events. First consideration is quality of selected data, to improve analysing and remove uncertainties quality of data is important. Second consideration is to select hadronic Z decays, to perform analysis on D_s meson is possible with selection of hadronic decays. In this chapter, these two considerations are discussed.

5.1 Data Quality

Event data is controlled many times to be selected for analysis. Recorded data by ECAL and TPC without any trouble is worth to be investigated. Angle between position of event and beam axis is taken account for event selection. If the angle is in the interval of 35° degree and 145° degree ($|\cos\theta| < 0.82$) associated event is considered as analysable. Sample polar angle distribution histogram of selected events are given in Figure 5.1.

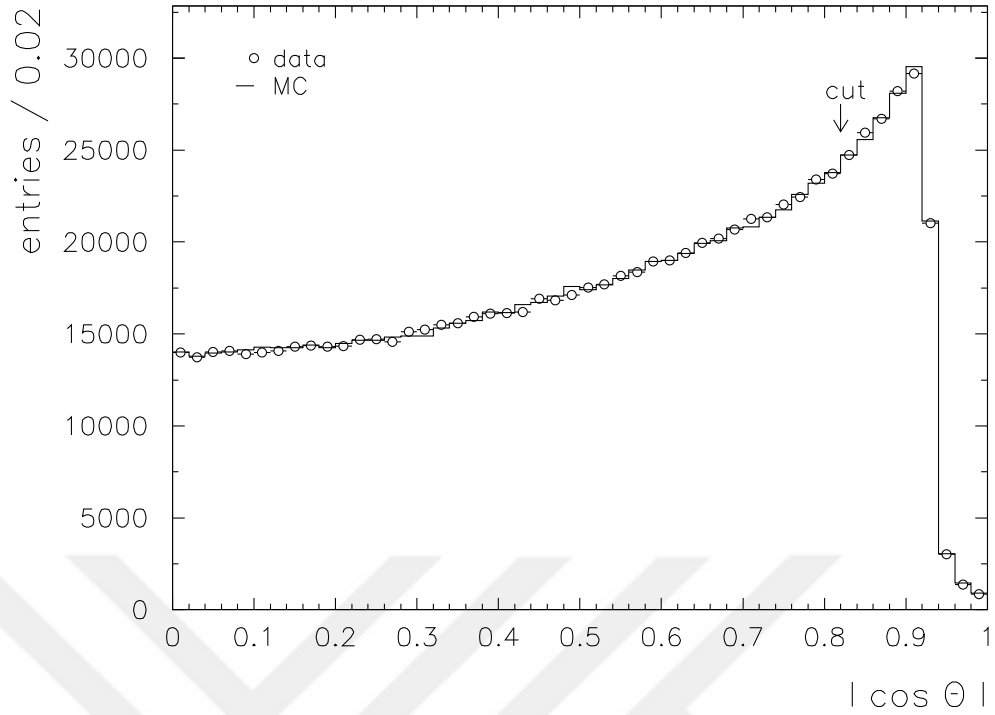


Figure 5.1 To ensure number of unnecessary data and raise quality level of analysing polar angle cut is applied to events. Angle of events between beam axis must be in interval of 35° degree and 145° degree to be selected for analysis.

5.2 Hadronic Event Selection

Decay channel of Z boson includes many type of particles. A quark-antiquark pair, lepton-antilepton pair or neutrino-antineutrino pair may be created after decay of Z boson. Even particles which can't be detected by detectors may be created. Frequently, creation of quark-antiquark is observed after decay. And as mentioned in Chapter 2 they turns into mesons and hadrons. To select data for analysing some cuts are applied to tracks and events.

5.2.1 Track Cuts

5 Restrictions are defined to select usable tracks. First restriction is defined for number of tracks in Time Projection Chamber. At least 4 coordinates must be recorded by TPC for analysing relevant track. Second restriction is defined for

polar angle. To select track for analyse, interval of polar angle is specified between 20° and 160° . Third restriction is defined for transverse impact parameters, d_0 . If the closest transversal distance between track and beam line is greater than 2 cm relevant track is not usable for analysing. Fourth restriction is defined for longitudinal impact parameters, z_0 . If distance between primary vertex and the point on the track used to evaluate d_0 in z -axis is greater than 5.0 cm, track is rejected. Last restriction is defined for transverse momentum, p_t . Tracks which has smaller transverse momentum value than 200 GeV, selection of track is cancelled.

5.2.2 Event Cuts

Two of conditions are ruled for events. First condition is number of selected tracks in an event. Every selected events must contain at least 5 charged tracks. Second condition is total energy of selected tracks in an event. If total energy of tracks in an event is greater than 15 GeV, event is selected. Two conditions must be satisfied together to be selected for analysing.

5.3 Event Background

After selection of events for analysing, a group of events are detected which are non-hadronic. Mostly, leptonic events are detected as non-hadronic events in selected events.

CHAPTER 6

ANALYSIS OF MONTE CARLO DATAS

6.1 Introduction

In this chapter, reconstruction of $D_s^\pm \rightarrow \pi^\pm + (\phi \rightarrow K^\pm)$ decay channel from Monte Carlo datas are mentioned. Selection of each of daughter and mother particles which contributes decay channel is made with respect to some criterias. This criterias are explained also in this chapter.

6.2 Modelling of Particles

In this analysis, the particles are modeled using the object oriented programming method. Each of particles are considered as an object. This is achieved by writing a particle class in C++. In this particle class, there are data members which keeps informations of particles. Informations which is taken from Monte Carlo and real data are added into data members of this particle class. Calculations about particle is made by the help of these informations. To made this calculations inside particle model, written particle class is inherited from TLorentzVector class. Relative calculations are achieved by help of this C++ class. TLorentzVector is developed in CERN, and helps making calculation of invariant mass, energy, momentum easily.

6.3 Particle Selection Criterias

While selecting particles, some criterias are considered for Monte Carlo data. This criterias are impact parameter, longitudinal impact parameter, momentum and ionisation energy loss respectively. Restrictions on this criterias is applied before selecting daughter and mother particles, and this restrictions improves purity and efficiency.

Threshold value is assigned for transverse impact parameter is 0.5 cm and longitudinal impact parameter is 2.0 cm. If the investigated track has greater value than 0.5 cm for impact parameter and has greater value than 2.0 cm for longitudinal impact parameter, research for investigated track is cancelled. For ionisation energy loss, assigned threshold value is 3.0 cm. If ionisation energy loss value for investigated track is smaller than -3.0 and greater than 3.0, relevant track is refused for investigating.

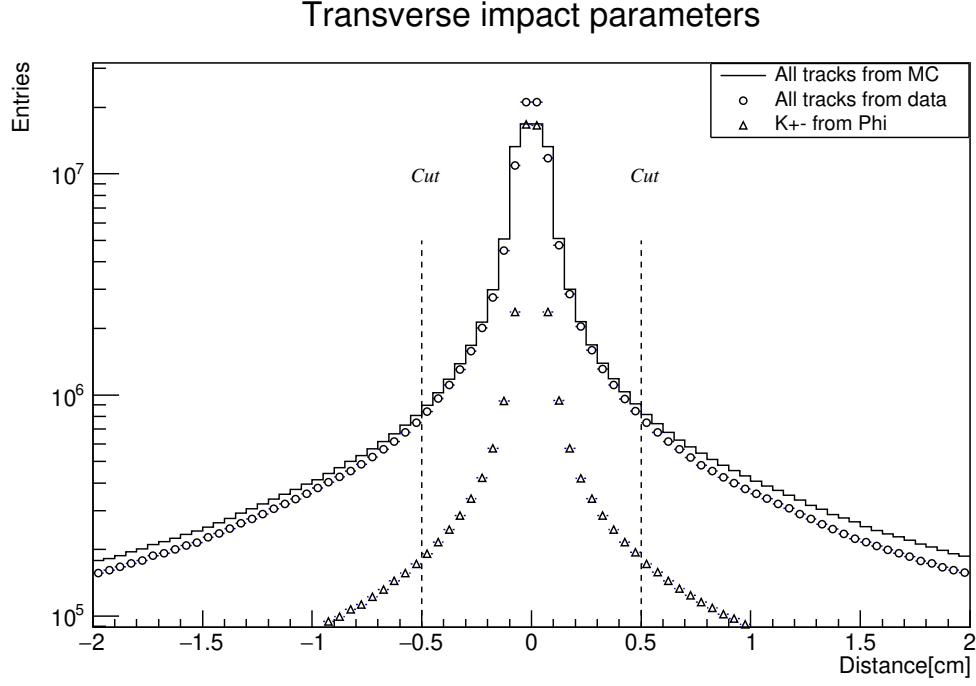


Figure 6.1 Transverse impact parameter distributions for reconstructed tracks from $\phi \rightarrow K^\pm$ decay. Dashed lines exist to indicate cut values.

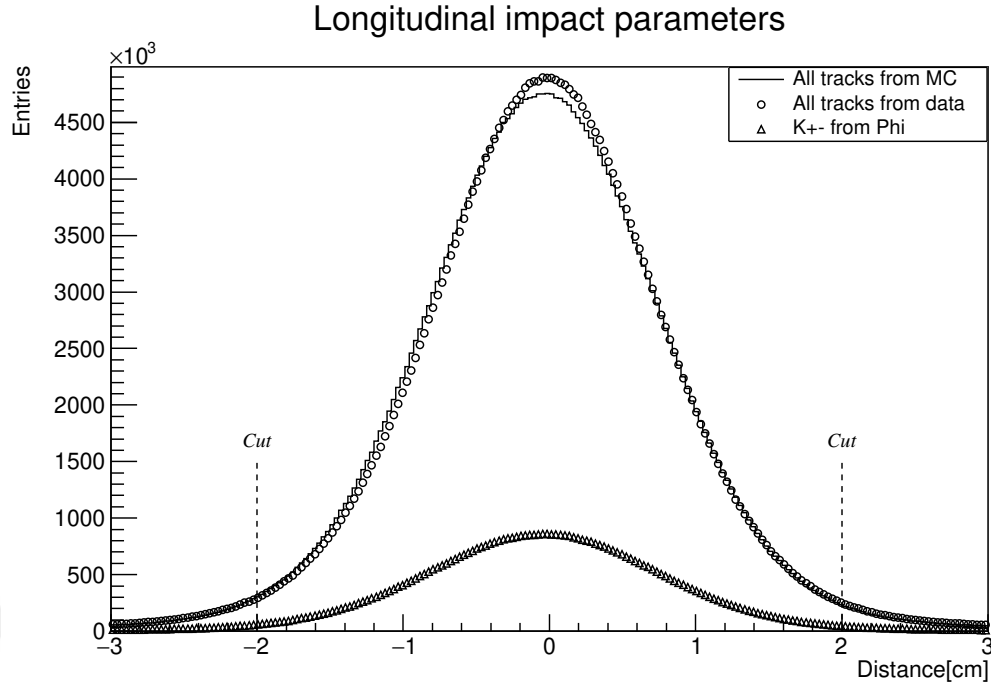


Figure 6.2 Longitudinal impact parameter distributions for reconstructed tracks from $\phi \rightarrow K^\pm$ decay. Dashed lines indicates applied cut.

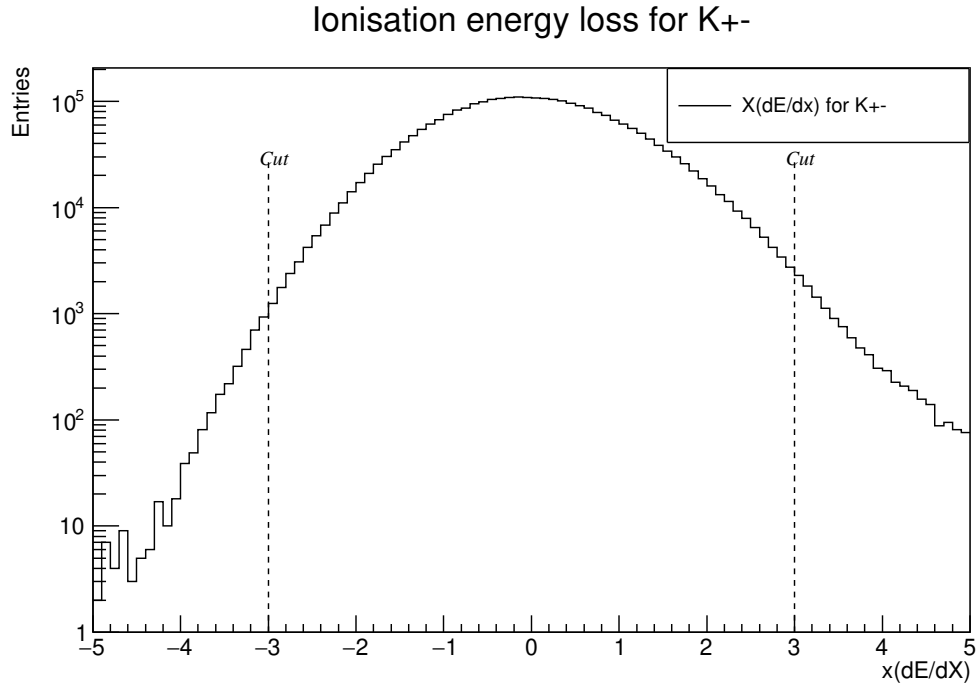


Figure 6.3 Histogram for ionisation energy loss for K^\pm .

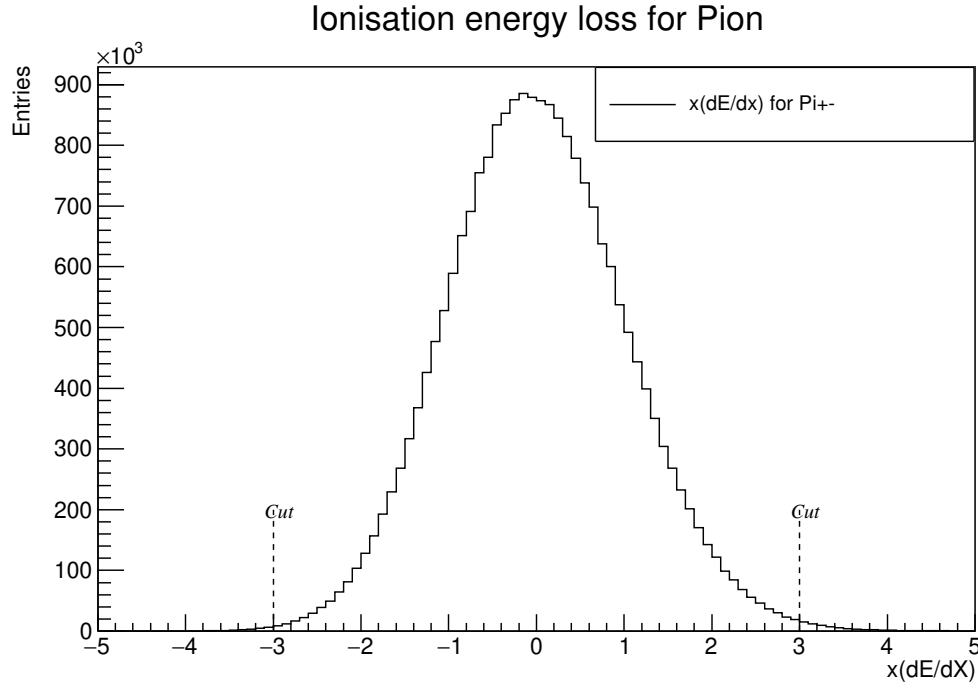


Figure 6.4 Histogram for ionisation energy loss for π^\pm .

Another selection criteria is momentum. This criteria can be considered as most important criteria for particle selection in this analysis. Threshold value for K^\pm particle is specified as 0.5 GeV. If investigated track has momentum value which is smaller than 0.5, this track is flagged as another particles trace rather than K^\pm and research for this track is skipped. Similarly, threshold value for π^\pm particle is specified as 1.0 GeV and if investigated track has a value which is smaller than 1.0 GeV, this track is not analysed.

6.4 Selection of K^\pm candidates

To achieve this, every track which is recorded per collision event is researched. K^\pm particle prototypes (models) are created. 4-momentum informations transverse impact parameter information, longitudinal impact parameter information, energy information are loaded to this particle prototypes from Monte Carlo data. And then, information of impact parameters, longitudinal impact parameters and value of ionisation energy loss are checked (Selection criterias). If selection criterias are satisfied, information of electrical charge, id, primary and secondary mother particle are loaded into particle prototype from Monte Carlo data. In here, from id, source particle of track can be identified, because this information is taken from simulation (Monte Carlo) data. After that, with respect to electrical charge

information K^\pm candidates are identified separately. End of these processes, K^\pm candidates are selected. To reconstruct decay channel, K^\pm particles which comes from decay of the Phi particle must be selected.

6.5 Creation of ϕ particle

Selected K^\pm are merged. As a result of this merging, a new particle is modelled, this particle is candidate of ϕ meson. Making calculation of invariant mass of ϕ meson candidate is required. This calculation is made from information of momentum and energy of ϕ candidate.

After making calculation of invariant mass, checking information of id and primary mother particle of selected K^\pm candidates is required. In here, mass of resultant Phi candidate is controlled. If modelled Phi candidates mass is smaller than 1.0 GeV, and greater than 1.05 GeV modelled Phi candidate is rejected. And end of this control, Phi particle is created successfully.

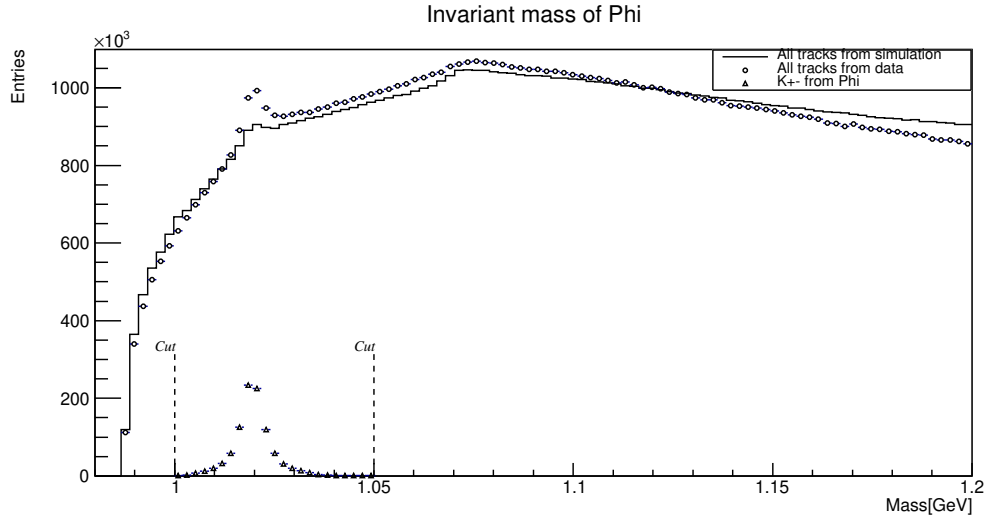


Figure 6.5 Mass histograms for ϕ particle. ϕ particle is created by merging K^\pm particles.

6.6 Selection of π^\pm particle

Selection of π^\pm candidates as same as selection of K^\pm s with small differences. π^\pm particle is modelled first. And momentum informations of current track is loaded into prototype of π^\pm . Checks for resultant momentum information

of prototype. After check for information of transverse impact parameter, longitudinal impact parameter and value of ionisation energy loss. If values for transverse impact parameter and longitudinal impact parameters are proper, id and primary mother particle information is taken from Monte Carlo data. Afterwards, π^\pm models which are used to reconstruct D_s meson with ϕ candidates are selected successfully.

6.7 Creation of D_s particle

Modelled pion candidates and created ϕ particles are merged to create D_s^\pm meson. In this phase id information of π^\pm , primary mother information of π^\pm and secondary mother of K^+ and K^- are checked. If reconstructed particles have satisfactory information, mass information of resultant D_s candidate is checked. If mass of D_s meson model is smaller than 1.8 GeV or greater than 2.1 GeV this model is rejected, else particle model is accepted as D_s meson.

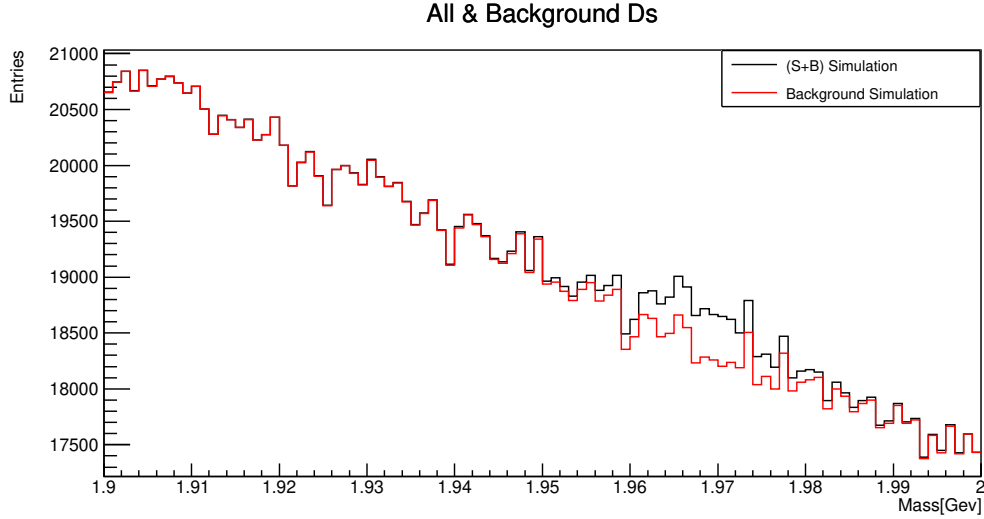


Figure 6.6 Mass distribution of all D_s models (Signal + Background) and rejected D_s models are plotted in this figure. Extraction of invariant mass distribution of D_s meson is achieved by the help of informations which are taken from Monte Carlo data.

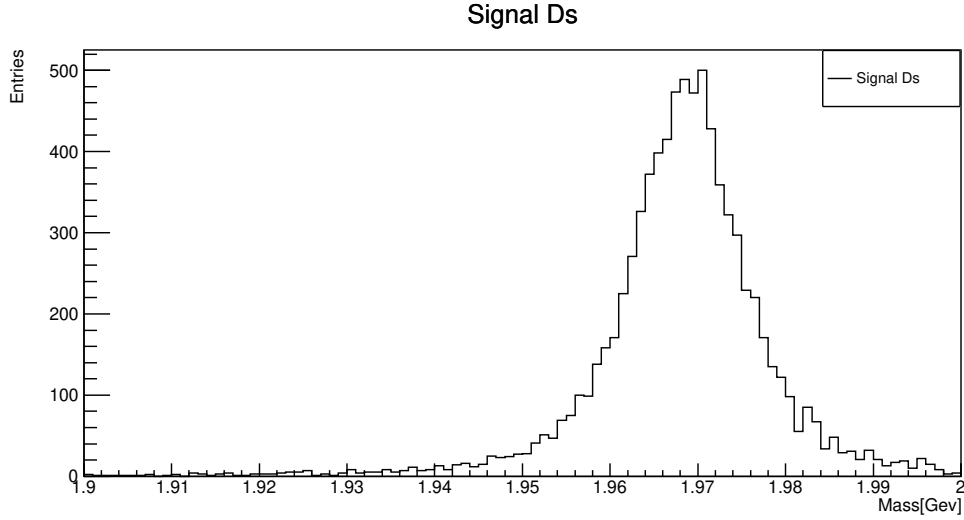


Figure 6.7 Invariant mass distribution of D_s meson. Each of this entries are invariant masses of accepted D_s . Mean value of the histogram is 1.969 GeV and invariant mass of D_s meson is 1.963 GeV.

6.8 Variables of Classification

Between situation of being signal or background of reconstructed D_s^\pm meson and some properties which belongs to reconstructed particles there are relations. Research on this informations is required, and most related properties must be selected. Values of this properties must be separable and groupable according to being single or background of reconstructed D_s^\pm meson. Selected properties are listed in below:

- Angle between ϕ and π^\pm particle
- Angle between K^+ and K^-
- Energy of reconstructed D_s^\pm
- Sum of energies of K^+ and K^-
- Angle between ϕ and K^+
- Angle between ϕ and K^-
- Angle between π^\pm and K^+
- Angle between π^\pm and K^-

These values are key to improve the purity of D_s mesons signal from real collision data. Because, ALEPH dont record information of first mother particle or information of second mother particle. Data of these properties are used in an artificial intelligence software kit to perform analysis on real data. Analysing on Monte Carlo data is machine learning portion of whole analysis. In next chapter, analysing real collision datas is explained.



CHAPTER 7

CLASSIFICATION, TEST AND FITTING

7.1 Introduction

In this chapter, classification of input variables, test of classification on real data and Monte Carlo data for obtaining D_s^\pm mesons invariant mass distribution, and fitting obtained histograms are explained. Additionally, software which is used in classification signal and background and determination of input variables and classification method are mentioned in this chapter. Conclusion essay can be found at the end of this chapter.

7.2 Separation Signal and Background

Data distribution of selected properties must be analyzed to examine the quality of selection. Before analysing real collision datas, this distribution is plotted.

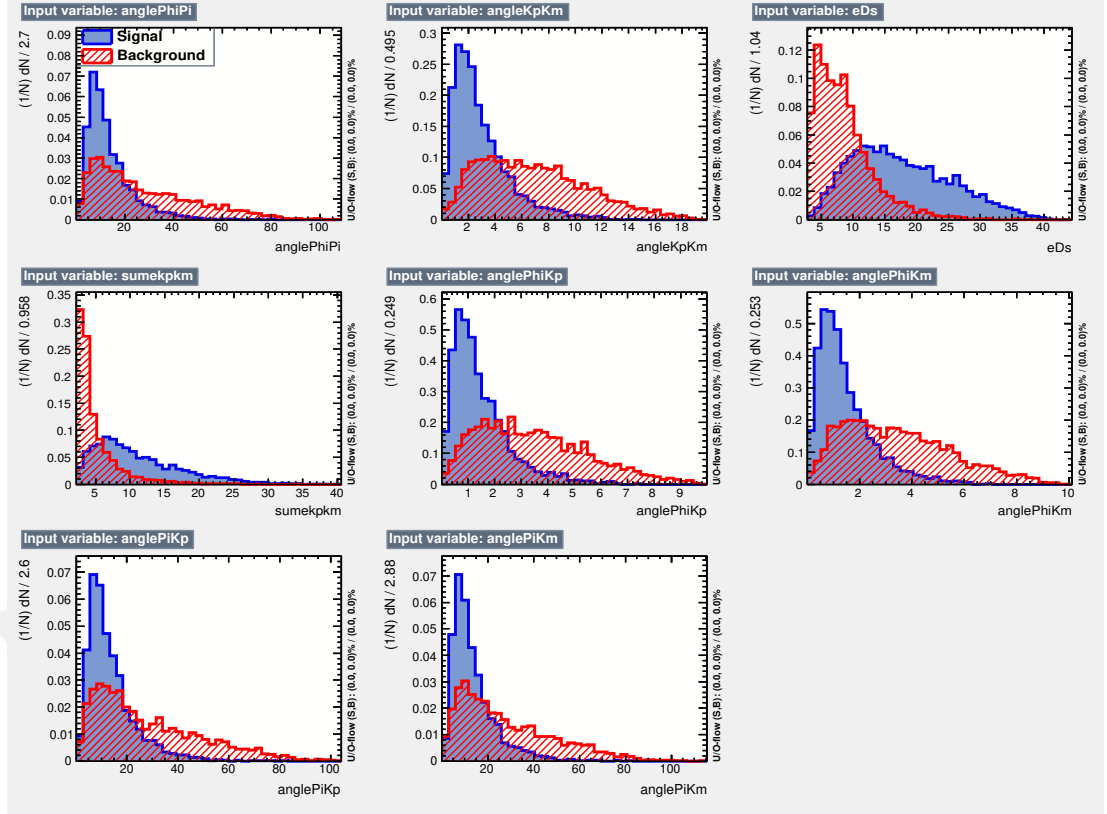


Figure 7.1 Signal and background distributions of selected variables. Situation of being signal or background of modelled D_s meson can be estimated by using these variables.

Plotting of distribution and classification are performed by TMVA toolkit. This toolkit is used for data analysis in high energy physics and operates under ROOT data analyse framework. Many of classification algorithms are included into TMVA. Also comparison between classification methods is available in TMVA Toolkit. Figure 7.2 shows comparison between classification methods which are included into TMVA Toolkit and optimum algorithm to classify signal and background.

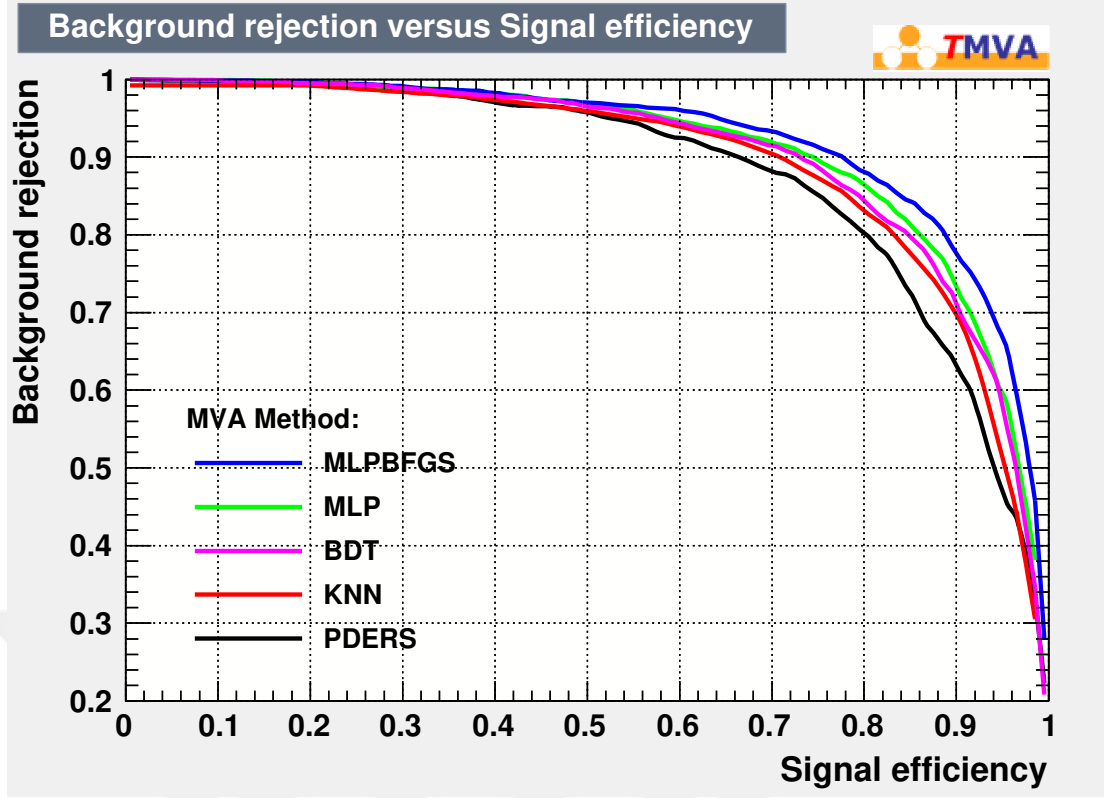


Figure 7.2 Performance graph of classification methods in TMVA. In TMVA, many of classification algorithms can be compared and this takes huge advantage for selection of optimum classification method.

In graph which is positioned above, x-axis represent signal efficiency which is defined as:

$$\epsilon_s = \frac{S_{selected}}{S_{total}} \quad (7.1)$$

and y-axis represent background rejection and this can be defined as:

$$1 - \epsilon_b = 1 - \frac{B_{selected}}{B_{total}} \quad (7.2)$$

As seen in figure, the best classification method to distinguish signal and background is assigned as MLPBFGS which is modified Multi Layer Perceptron. But making classification with this method consumes a lot of time. Faster method is required for this analyse because number of events are more than millions. Due to this requirement, BDT is assigned as optimum classification method, and classification in this analysis is made with BDT method. BDT is one of the supervised machine learning algorithms. After making classification with BDT method, TMVA evaluates cut efficiency for selected method. Cut efficiency value can be learned from two of graphs which is plotted by TMVA.

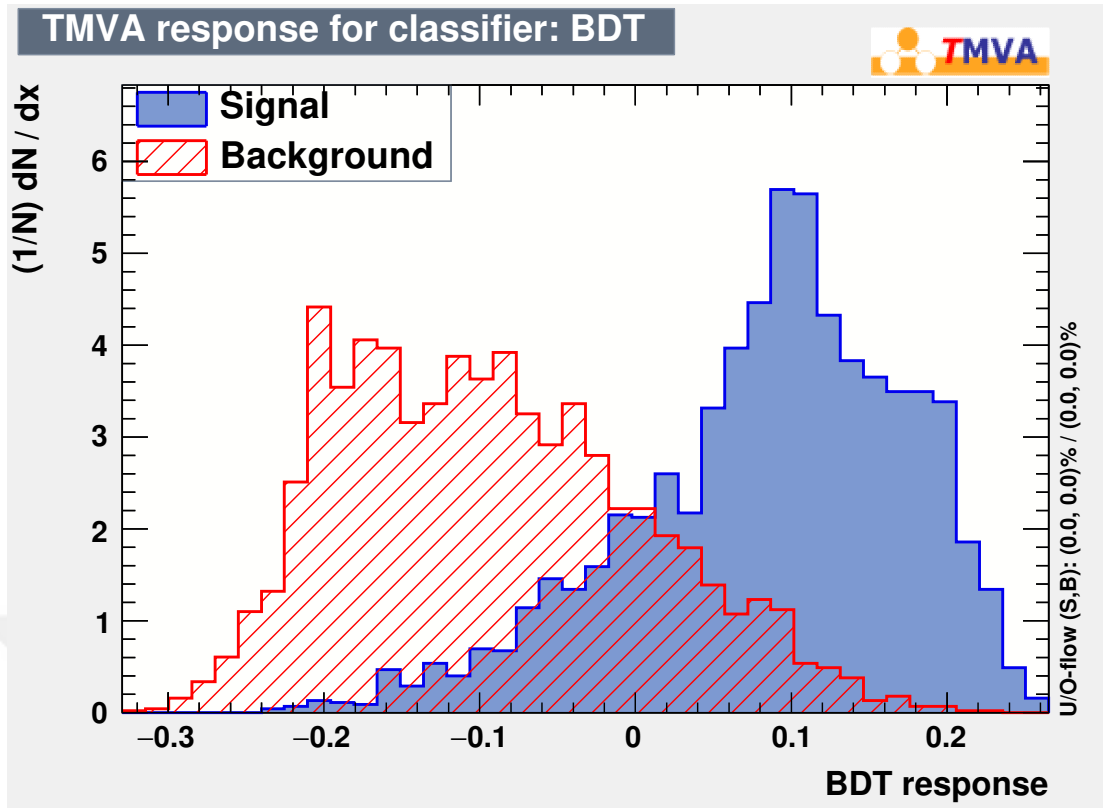


Figure 7.3 Classifier response distribution for BDT method.

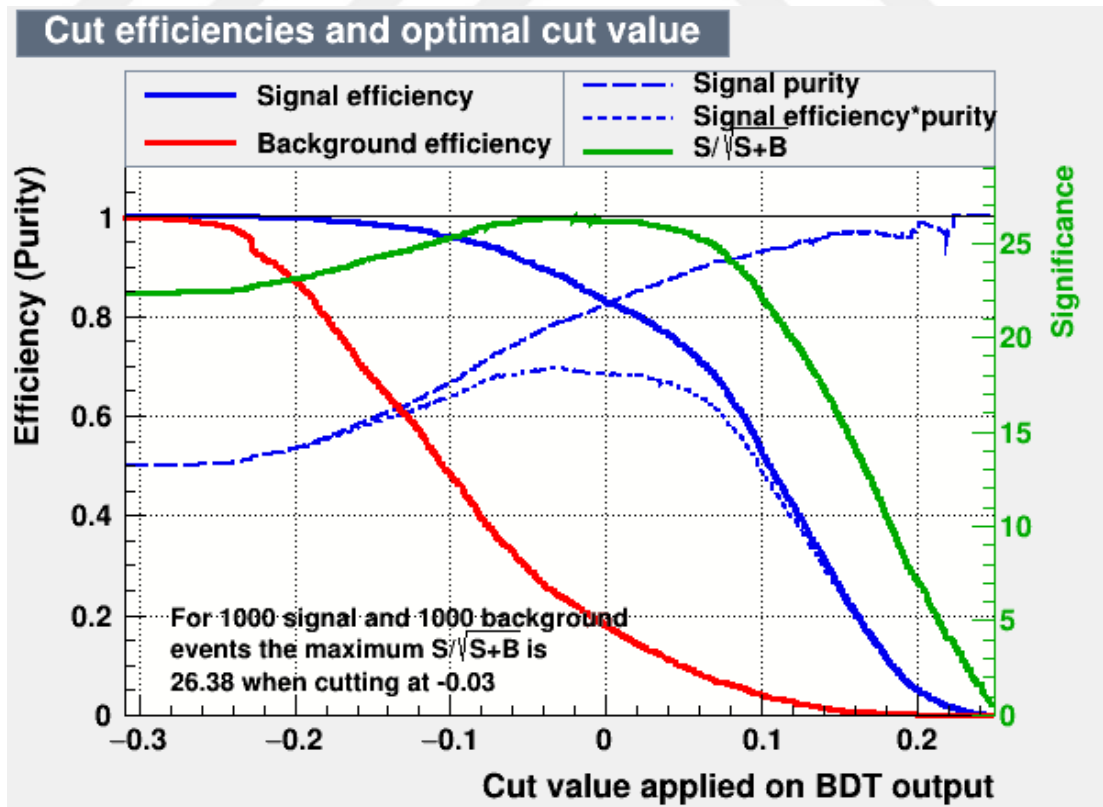


Figure 7.4 Cut efficiency distribution for BDT method.

Maximum efficient value for BDT method is calculated as -0.02 by TMVA. Also weights of input variables are calculated by TMVA, and impact of input variables on being signal or background is evaluated. Weights are expressed as fractional numbers and weights specifies the effect of selected properties on being signal or background of reconstructed D_s^\pm meson. By using weight values real data can be analysed.

7.3 Testing Real Data

After making classification, real collision can be tested. In this phase, almost whole process is same with the processes of Monte Carlo analysis. Reconstruction of particles are achieved by the same way. Difference between Monte Carlo data analyzing process and real collision data analyzing process is absence of specific informations which is taken from Monte Carlo datas. In this case, calculated weight informations which is produced after classification are used. After making classification, calculated weights of input variables are stored in an XML file. And this file included into test software to make test. Resultant histograms are added below.

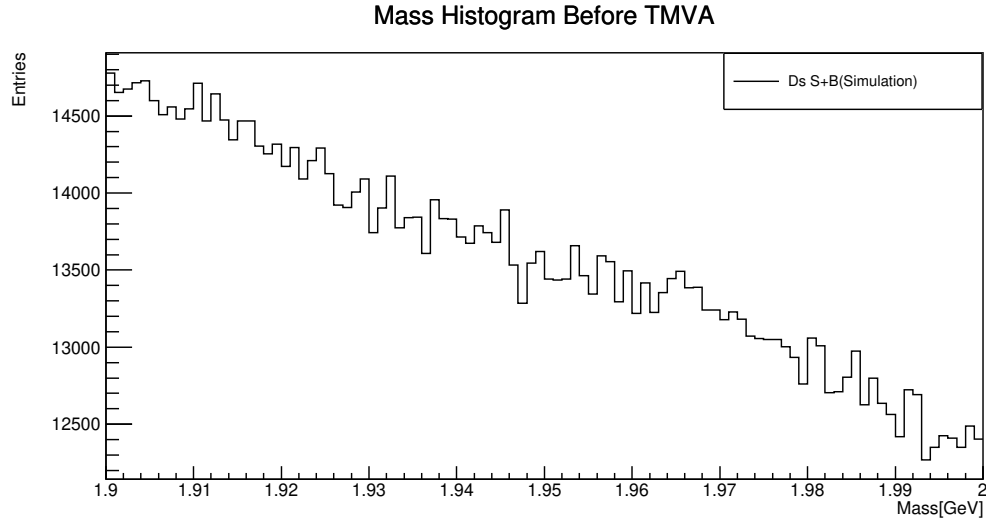


Figure 7.5 Histogram for mass all D_s meson models. Invariant mass distribution of D_s meson is not significant in this histogram, classification of signal and background is required.

Table 7.1 Calculated numbers of Signal, Background, Efficiency and Purity before and after TMVA.

	Signal	Background	S/B	Purity	Efficiency	Eff. x Pur.
Before	7160	1934530	0.00370115	0.00368751	1	0.00368751
After	6377	496592	0.0128415	0.0126787	0.890642458	0.01129218853

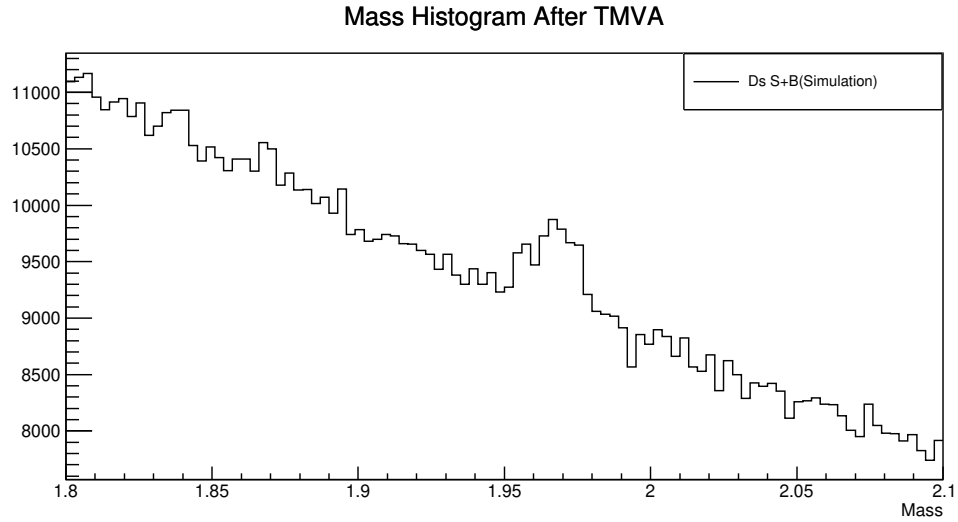


Figure 7.6 Histogram for mass of all D_s meson models after making classification. Significance is improved by help of classification, identification of D_s^\pm mesons signal from huge data is performed.

After making classification, backgrounds are rejected mostly, but also some of signal are lost after testing on real data. Results are listed in table below.

7.4 Testing Monte Carlo Data

Monte Carlo datas are also tested after classification. Despite, analyse of Monte Carlo datas is performed with certain information, to examine classification this test is made. Before test, there are 5837126 entries in background histogram of invariant mass of D_s^\pm meson. After test there are 1461470 entries remained. Signal histogram has 7231 events before test. After test, entry number decreased to 6446.

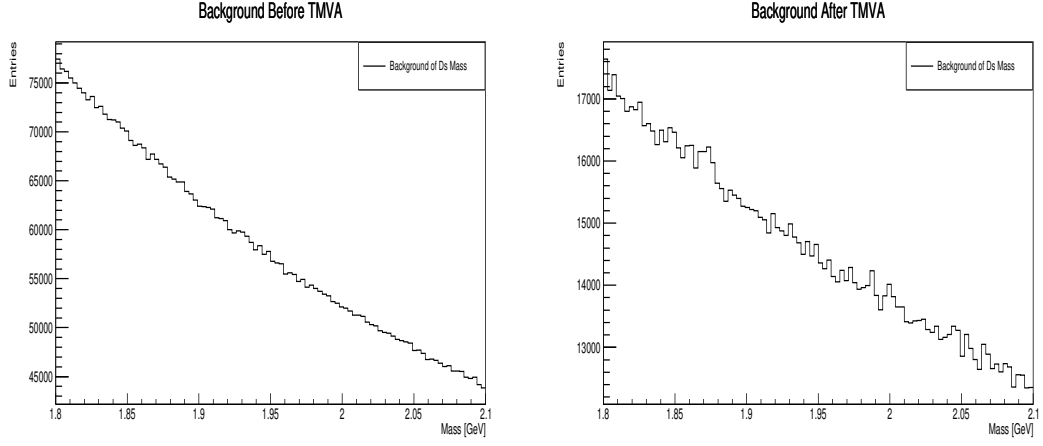


Figure 7.7 Mass histograms for background of D_s meson models after making classification. After TMVA appearance of histogram which is positioned in right side is changed.

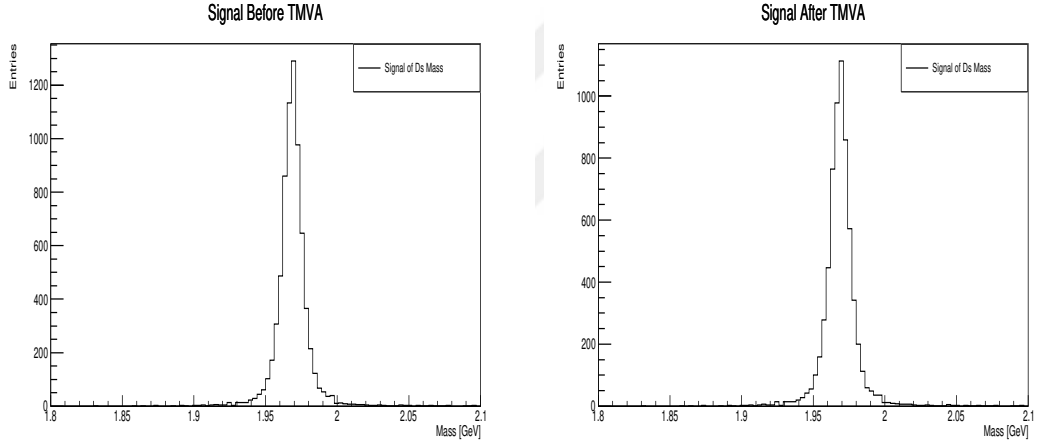


Figure 7.8 Invariant mass distribution (signal) of D_s meson. These histograms are plotted after making of classification.

7.5 Analysis for Different Energy Levels

To detect more efficient energy interval, whole analysis is repeated for 5 different energy levels. Obtained histograms are added below.

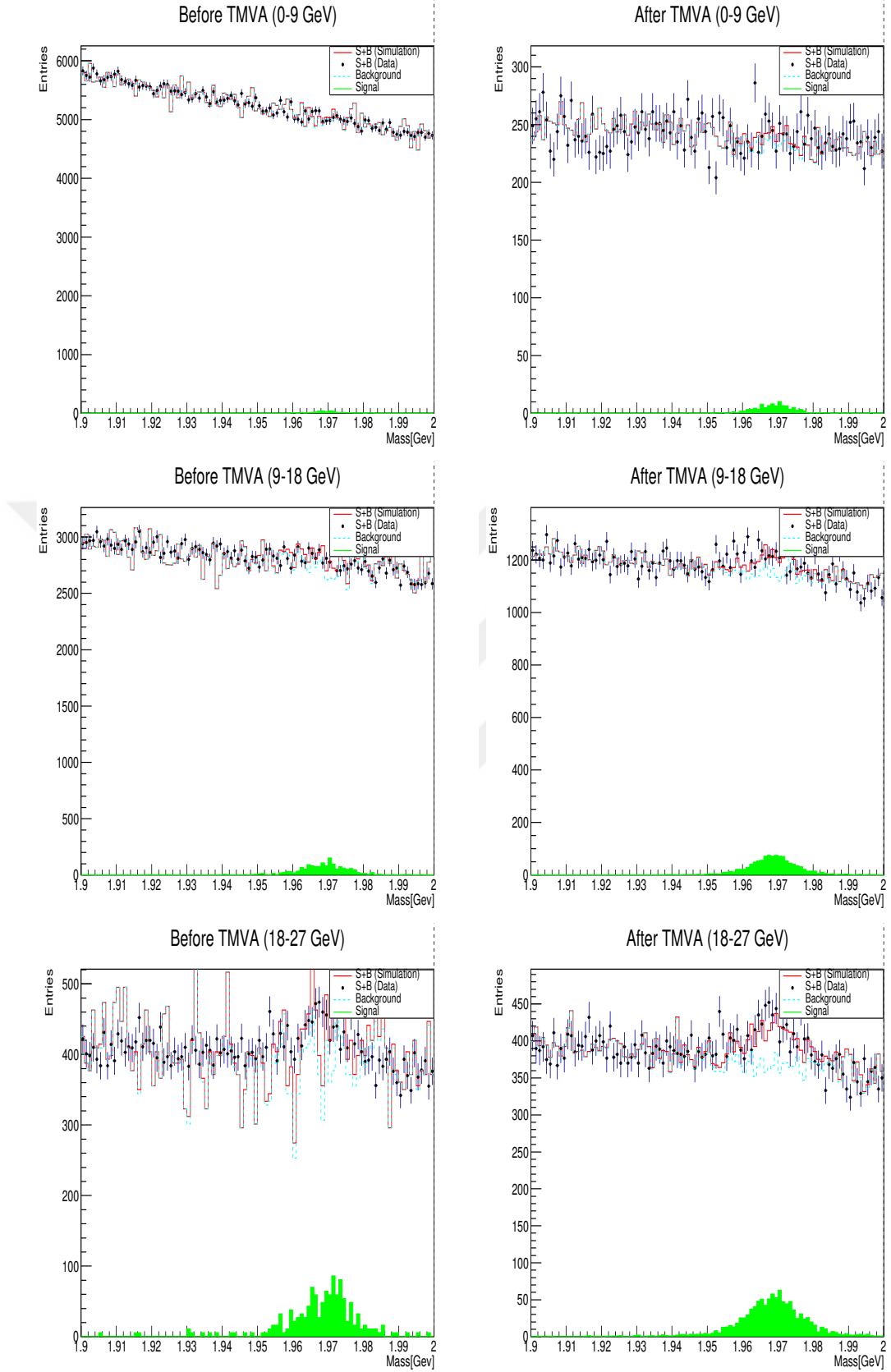


Figure 7.9 Plotted histograms for different energy levels (1).

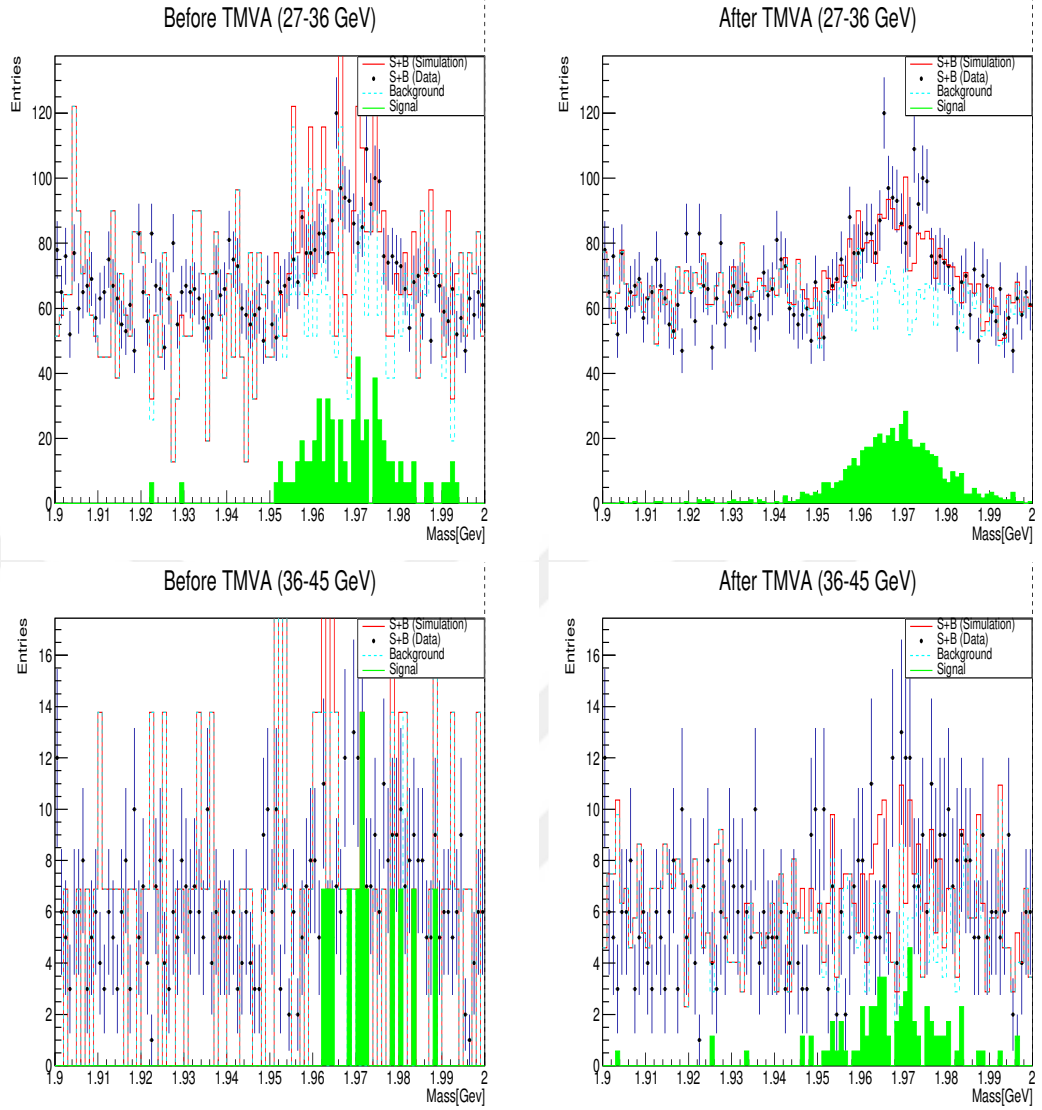


Figure 7.10 Plotted histograms for different energy levels (2).

Table 7.2 Calculated numbers of Signal, Background, Efficiency and Purity for real data before and after TMVA.

	Signal	Background	S/B	Purity	Efficiency	Eff. x Pur.
Before	11650	896296	0.0129	0.0128	1	0.0128
After	5250	302649	0.0173	0.310	0.450	0.139

7.6 Fitting

In this section, fitting for signal and background for both Monte Carlo and real data is explained briefly.

7.6.1 Signal Fitting

Signal which is extracted from Monte Carlo datas, is essentially parametrized as below:

$$f(x) = A_1 e^{\left(\frac{-1}{2}(x-A_2)^2/A_3^2\right)} \quad (7.3)$$

Signal shape is similar to gaussian distribution. Here, A1 stands for height of the curve, A2 stands for mean value (close to invariant mass), and A3 stands for width of the curve (standard deviation).

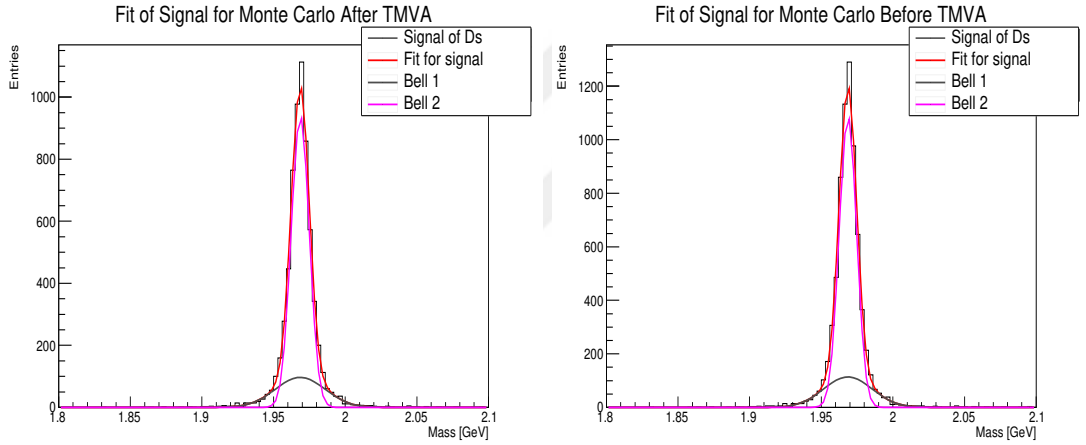


Figure 7.11 Fitting of two signal histogram. Signal is fitted to two gaussian functions.

7.6.2 Background Fitting

Background distribution is modelled as a 2nd degree polynomial function, and parametrized as follows:

$$f(x) = A_0 x^2 + A_1 x + A_2 \quad (7.4)$$

where A_0, A_1 and A_2 are free parameters.

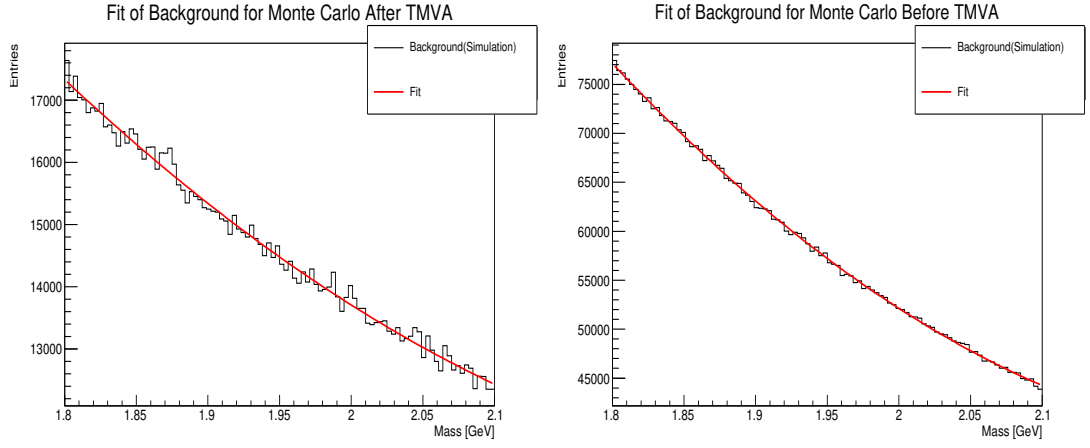


Figure 7.12 Fitting of two background histogram. Histogram can be fitted to second degree polynomial equation easily.

7.6.3 Total Distribution Fitting

Total distribution is parametrized as sum of a 2nd degree polynomial function and two of gaussian function

$$f(x) = A_0x^2 + A_1x + A_2 + A_3e^{\left(\frac{-1}{2}(x-A_4)/A_5(x-A_4)/A_5\right)} + A_6e^{\left(\frac{-1}{2}(x-A_4)/A_7(x-A_4)/A_7\right)} \quad (7.5)$$

Here A_0 , A_1 and A_2 are parameters for polynomial portion. A_3 , A_4 , A_5 , A_6 and A_7 are parameters for gaussian portion.

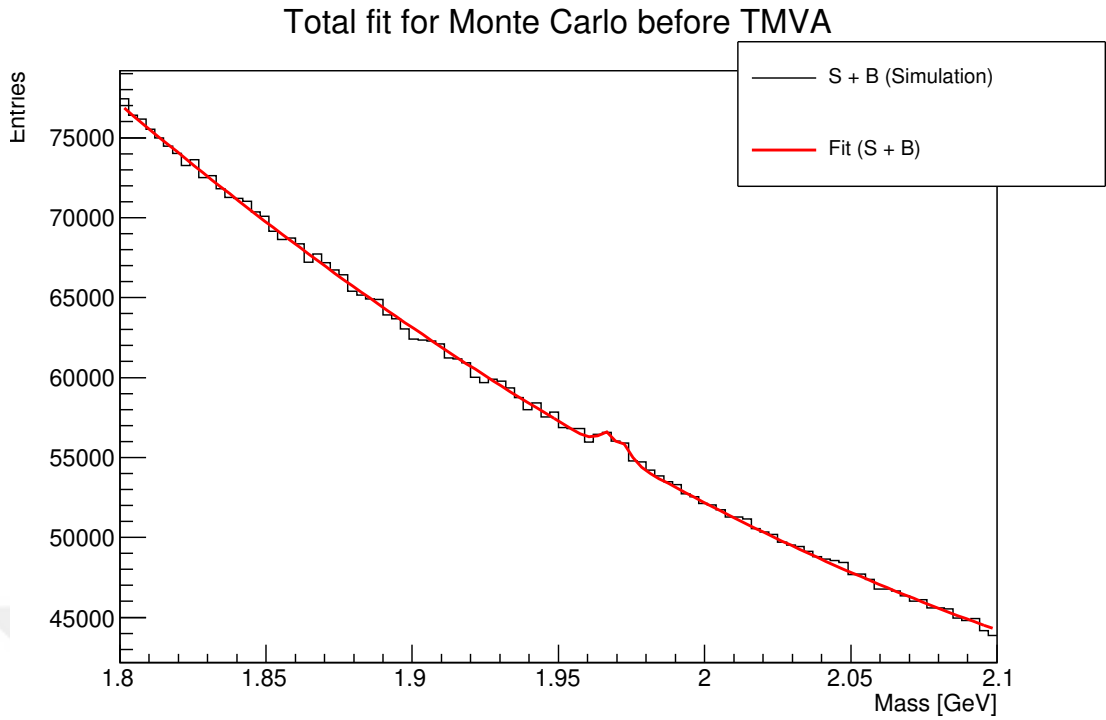


Figure 7.13 Total mass distribution of D_s candidates. Invariant mass distribution of D_s meson is not obvious.

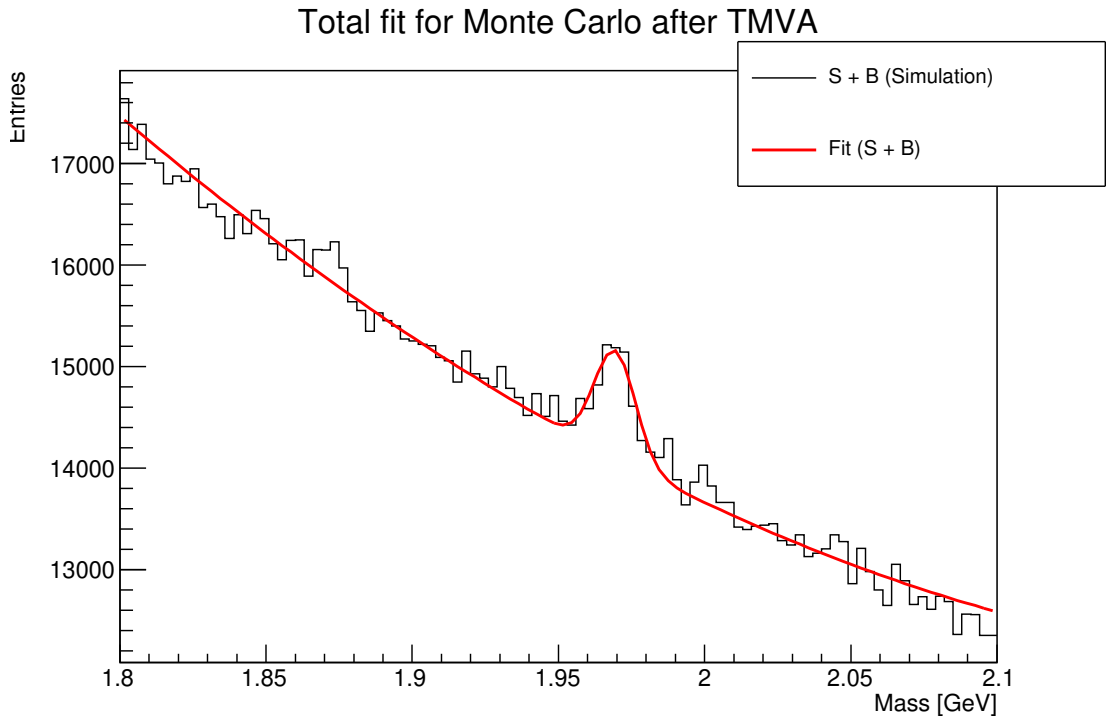


Figure 7.14 Total mass distribution after classification. Signal of D_s meson is more obvious after classification.

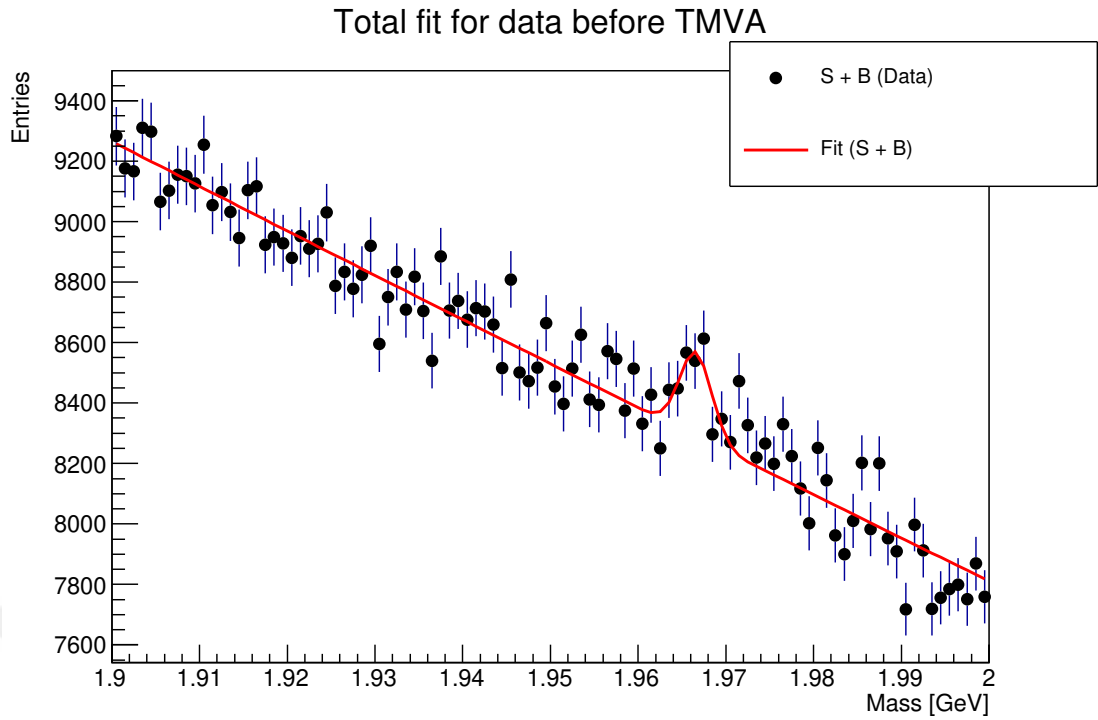


Figure 7.15 Total mass distribution for real data before classification.

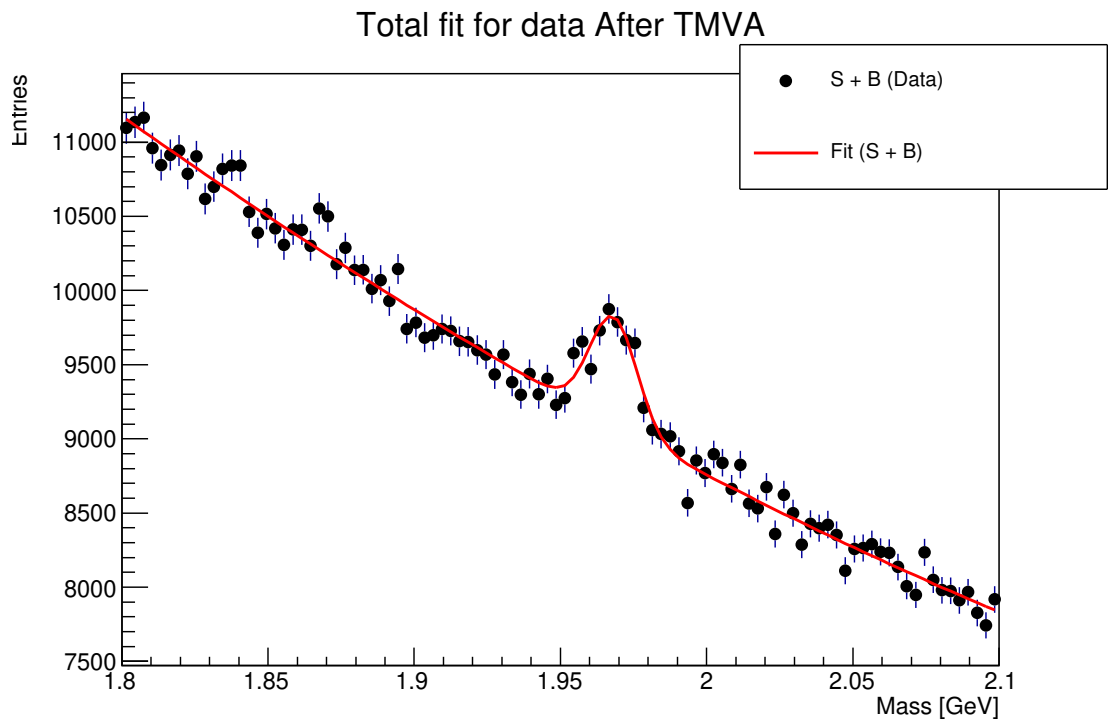


Figure 7.16 Total mass distribution for real data after classification. Most of background entries are rejected after classification.

7.7 Conclusion

Each of particles which exist in decay channel of $D_s \rightarrow \pi^\pm + [\phi \rightarrow K^+ + K^-]$ are modelled. Informations for properties of particles are taken from Monte Carlo datas which are produced by event generator softwares. These informations are loaded to particle models. By reconstructing decay channel, invariant mass distribution of D_s^\pm meson is obtained and plotted. Monte Carlo datas are assumed as guide. For detecting D_s^\pm mesons signal without using certain informations from Monte Carlo datas, from real collision datas, properties of modelled particles which are help to reconstruct D_s^\pm meson are selected. Values of these properties are recorded to classify signal and backgrounds with TMVA. Many of classification algorithms are compared to select the optimum classification algorithm. BDT is founded as the optimum algorithm to classify signal and background. Purifying of signals in real datas are improved, with some losses on signals. Backgrounds are mostly rejected. By the end of this analysis, invariant mass distribution of D_s^\pm meson is extracted from real collision datas. Results of fitting to data, before and after applying TMVA (Table 7.2) shows that the signal significance, measured as the product of efficiency and signal purity, improves greatly. Importance of machine learning algorithms for these type of analysis is proved.

7.7.1 Outlook

By applying same analysing procedure, invariant mass distribution of any of known particle with its decay channel can be analysed. Exploring new particles with machine learning algorithms is also possible, but theoretical information about wanted particle is very important to model the particle, to reconstruct decay channel of wanted particle by the help of software. This analysing technique is not proper for only high energy physics. In other disciplines like statistics, medicine data analysing is performed. Many of problems can be solved by data analysing. Data analysing is common point for many disciplines.

REFERENCES

- [1] Myers, S., Picasso, E. (2006). The design, construction and commissioning of the CERN large Electron Positron collider, *Contemporary Physics*. **31(6)**: 387403. doi:10.1080/00107519008213789. ISSN 0010-7514.
- [2] Gell-Mann, M. (1964). A Schematic Model of Baryons and Mesons, *Physics Letters*. **8(3)**: 214–218.
- [3] Zweig, G.(1964). An SU(3) Model for Strong Interaction Symmetry and its Breaking *Developments in the Quark Theory of Hadrons*, pp 22-101 CERN-TH-401.
- [4] Sodickson, L., Bowman, W., Stephenson, J., Weinstein, R. (1970). Single-Quantum Annihilation of Positrons, *Physical Review*.124(6): 18511861.
- [5] Glashow, S. (1959). The renormalizability of vector meson interactions, *Nucl. Phys.***10**, 107.
- [6] Weinberg, S. (1967). A Model of Leptons(PDF). *Phys. Rev. Lett.* **19**: 1264-66.
- [7] Salam, A., Ward, J. C. (1959). Weak and electromagnetic interactions, *Nuovo Cimento*. **11(4)**, 568-577.
- [8] Field R. D. and Feynman R. P. (1978). A Parameterization of the properties of Quark Jets, *Nucl. Phys.* **B 136 1**.
- [9] Barger, V.; Phillips, R. (1997). *Collider Physics*.
- [10] Greensite, J. (2011). *An introduction to the confinement problem*. Lecture Notes in Physics.821.
- [11] Gadzicki, Marek; Gorenstein, Mark I. (2016), Rafelski, Johann (ed.), *Hagedorns Hadron Mass Spectrum and the Onset of Deconfinement, Melting Hadrons, Boiling Quarks From Hagedorn Temperature to Ultra-Relativistic Heavy-Ion Collisions at CERN*. Springer International Publishing, pp. 87-92.
- [12] Increasing LEP's energy from 90 to 140 GeV (1995). Intl: <https://timeline.web.cern.ch/increasing-leps-energy-90-140-gev>, 15.12.1995.

- [13] Synchrotron. Intl: <https://byjus.com/physics/synchrotron>
- [14] Introduction to the ALEPH Experiment Intl: <http://aleph.web.cern.ch/aleph/aleph/newpub/intro.html>, 30.04.1999.
- [15] J. Knobloch and P. Norton. (ALEPH Collab.) (1996). Status of Reconstruction Algorithms for ALEPH. *Draft ALEPH notes*.
- [16] T. Sjöstrand (1994). *High-energy-physics event generation with PYTHIA 5.7 and JETSET 7.4* *Comp. Phys. Com.* V 82. 74-89.

CURRICULUM VITAE

Name: Mustafa Koşmaz

Occupation

(2014 - 2015) Anatolia Yazılım-Junior Software Developer.

(2018) 5 Adım Yazılım-Junior Software Developer. (2 Months)

Education

(2018) B.Sc. degree in Engineering Physics in Gaziantep University.

(2009) Computer Technologies and Programming in Adana Vocational School
Çukurova University.

Language

English Intermediate (B1)

Conferences Attended

(27 February 2021) USBIK Natural Sciences Conference.